Molecular Cell

Article

Active growth signaling promotes senescence and cancer cell sensitivity to CDK7 inhibition

Graphical abstract

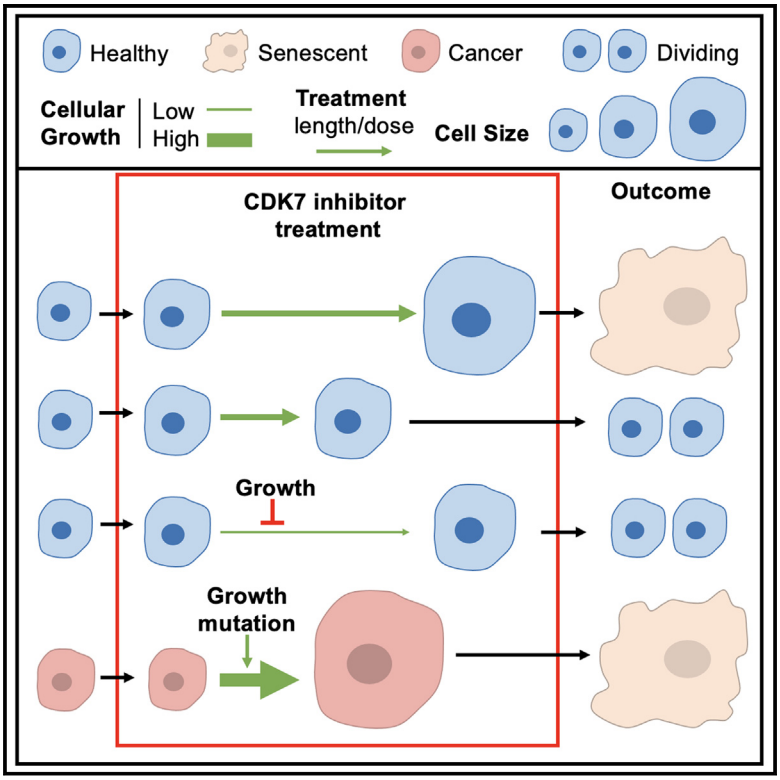

Highlights

- CDK7 inhibition drives an irreversible cell-cycle exit by inducing a senescent state
- CRISPR screen identifies mTOR signaling as key determinant of CDK7i sensitivity
- CDK7i-induced senescence largely depends on active mTOR growth signaling
- Cancer-associated growth signaling increases sensitivity to CDK7 inhibitor

Authors

Gemma A. Wilson, Karla Vuina, Georgina Sava, ..., Simak Ali, Cosetta Bertoli, Robertus A.M. de Bruin

Correspondence

r.debruin@ucl.ac.uk (R.A.M.d.B.), c.bertoli@ucl.ac.uk (C.B.)

In brief

Wilson et al. show that enhanced growth rate, a hallmark of cancer, plays a key role in a cells' sensitivity to CDK7 inhibition, by driving a permanent cell division arrest via increasing cell size beyond a point of no return. This work can guide the use of CDK inhibitors in the clinic.

Wilson et al., 2023, Molecular Cell *83*, 4078–4092
November 16, 2023
https://doi.org/10.1016/j.molcel.2023.10.017

CellPress

CellPress
OPEN ACCESS

Molecular Cell

Article

Active growth signaling promotes senescence and cancer cell sensitivity to CDK7 inhibition

Gemma A. Wilson,[1,8] Karla Vuina,[1,8] Georgina Sava,[2] Caroline Huard,[3] Leticia Meneguello,[1,4] Jasmin Coulombe-Huntington,[3,5] Thierry Bertomeu,[3] Rory J. Maizels,[1] Josh Lauring,[6] Janos Kriston-Vizi,[1] Mike Tyers,[3,7] Simak Ali,[2] Cosetta Bertoli,[1,9,*] and Robertus A.M. de Bruin[1,4,9,10,*]

[1]Laboratory for Molecular Cell Biology, University College London, London, UK
[2]Division of Cancer, Department of Surgery & Cancer, Imperial College London, London, UK
[3]Institute for Research in Immunology and Cancer, Université de Montréal, Montréal, QC, Canada
[4]UCL Cancer Institute, University College London, London, UK
[5]Department of Bioengineering, McGill University, Montréal, QC, Canada
[6]Janssen Research and Development, the Sidney Kimmel Comprehensive Cancer Center at Johns Hopkins, Baltimore, MD, USA
[7]Hospital for Sick Children, University of Toronto, Toronto, ON, Canada
[8]These authors contributed equally
[9]Senior author
[10]Lead contact
*Correspondence: r.debruin@ucl.ac.uk (R.A.M.d.B.), c.bertoli@ucl.ac.uk (C.B.)
https://doi.org/10.1016/j.molcel.2023.10.017

SUMMARY

Tumor growth is driven by continued cellular growth and proliferation. Cyclin-dependent kinase 7's (CDK7) role in activating mitotic CDKs and global gene expression makes it therefore an attractive target for cancer therapies. However, what makes cancer cells particularly sensitive to CDK7 inhibition (CDK7i) remains unclear.

Here, we address this question. We show that CDK7i, by samuraciclib, induces a permanent cell-cycle exit, known as senescence, without promoting DNA damage signaling or cell death. A chemogenetic genome-wide CRISPR knockout screen identified that active mTOR (mammalian target of rapamycin) signaling promotes samuraciclib-induced senescence. mTOR inhibition decreases samuraciclib sensitivity, and increased mTOR-dependent growth signaling correlates with sensitivity in cancer cell lines. Reverting a growth-promoting mutation in *PIK3CA* to wild type decreases sensitivity to CDK7i. Our work establishes that enhanced growth alone promotes CDK7i sensitivity, providing an explanation for why some cancers are more sensitive to CDK inhibition than normally growing cells.

INTRODUCTION

The main driver of cell-cycle progression is cyclin-dependent kinase (CDK) activity and increased CDK activity has been widely reported in various cancers, making them attractive targets for new treatments.[1] Several studies have shown a marked sensitivity of many cancer types to selective CDK7 inhibition.[2] CDK7 is the main CDK activating kinase (CAK), which, by phosphorylating and fully activating the main cell-cycle-dependent CDKs, CDK1, 2, 4, and 6, supports cell-cycle progression. In addition to its role in CDK activation, CDK7 is also required for RNA polymerase II (RNA Pol II)-dependent transcription, through RNA Pol II and CDK9 phosphorylation.[3]

Cancer cells are sensitive to CDK7 inhibitors at doses at which healthy cells are insensitive, suggesting that treatments might be well tolerated in a clinical setting.[3] Inactivation of CDK7 results in loss of activation of all mitotic CDKs and is therefore expected not only to prevent cell-cycle entry and progression, but also to directly promote cell-cycle exit. This suggests that CDK7 inhibitors could trigger cell-cycle exit in cancers with either mutations in proteins involved in cell-cycle exit (p16/ATM-p53-p21) and/or cell-cycle entry pathways (Ras-Raf-Mek-Erk-c-Myc-CyclinD/CyclinE-Rb-E2F), potentially benefiting a wide range of patients. Additionally, with many cancers depending on transcriptional drivers, CDK7 inhibitors could hit two birds with one stone: the continued cell-cycle progression via CDK inhibition and the addiction to transcriptional drivers via RNA Pol II inhibition.

Samuraciclib is a recently developed non-covalent, ATP-competitive, selective CDK7 inhibitor. It has been shown to inhibit proliferation of multiple cancer cell lines at lower concentrations than non-tumorigenic cell lines and to significantly inhibit tumor growth in a mouse colon cancer xenograft model, with no major side effects. Samuraciclib is currently in several phase I/II clinical trials, sometimes under the name CT7001 or ICEC0942.[4] Importantly, the US Food and Drug Administration (FDA) has

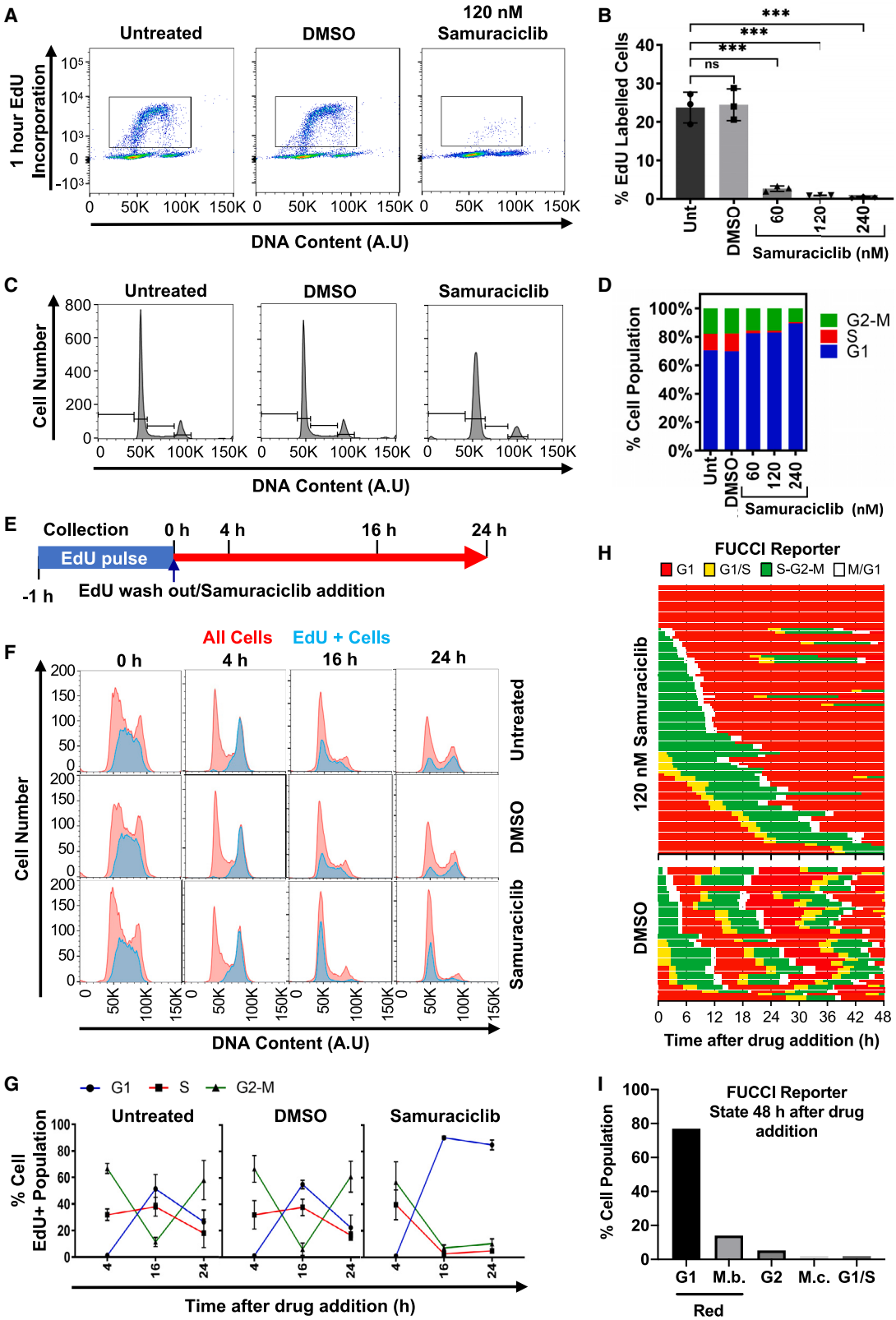

(legend on next page)

granted Fast Track designations to samuraciclib in combination with fulvestrant for CDK4/6i-resistant Hormone Receptor+, HER2− advanced breast cancer and samuraciclib in combination with chemotherapy for the treatment of locally advanced or metastatic triple negative breast cancer.[5] With samuraciclib and other CDK7 inhibitors moving ever closer to the clinic, a more fundamental understanding of what determines sensitivity to CDK7 inhibition is required to optimize the efficacy of these treatments and guide patient stratification.

In this study we investigate how CDK7 inhibition, via samuraciclib treatment, affects cell-cycle entry, progression, and exit and the fundamental cellular processes that determine CDK7i sensitivity. Our data show that samuraciclib acutely arrests cells in a G1 state of the cell cycle without activating the DNA damage response, which over time leads to senescence. Through a chemogenetic genome-wide CRISPR knockout (KO) screen, we identified growth, through mTOR (mammalian target of rapamycin) signaling, as an important determinant of samuraciclib-induced senescence. Our data suggest that cancer-associated mutations known to drive cellular growth could be indicative of CDK7i sensitivity and therefore a potential marker to direct their use in the clinic.

RESULTS

Samuraciclib inhibits cell proliferation and induces cell-cycle arrest in G1

CDK7 is the major CAK, phosphorylating CDK1, 2, 4, and 6, the main cell-cycle-dependent CDKs. CDK7 inhibition is therefore expected to prevent cell-cycle entry and progression and promote cell-cycle exit. The selective CDK7 inhibitor samuraciclib has been shown to be largely cytostatic, inhibiting cancer cell proliferation and tumor growth.[3] However, other less selective CDK7 inhibitors, such as THZ1, have been reported to significantly increase cell death, which has largely been attributed to their effect on inhibition of transcription.[3,6,7] To understand how selective CDK7 inhibition, by samuraciclib, affects cell-cycle progression, we used the non-transformed retinal pigment epithelial cell line RPE1, which retain intact cell-cycle checkpoints. The SRB (sulforhodamine B colorimetric) assay, which measures cellular protein content,[8] was used to assess cell number upon samuraciclib treatment and established a GI_{50} of 120 nM (Figure S1A). This was confirmed by an assay based on cellular metabolic activity, the MTT (3-(4,5-dimethylthiazol-2-yl)-2,5-diphenyl-2H-tetrazolium bromide) viability assay[9] using half, full, and double GI_{50} samuraciclib concentrations for 48 h (Figure S1B). At 120 nM of samuraciclib, we observed both a reduction in phosphorylation of the C-terminal domain of RNA Pol II and of the T-loop of CDK1, which are both known to be carried out by CDK7 (Figure S1C).

To confirm previous studies that show that selective CDK7 inhibition does not increase cell death[3] to the extent reported for the less selective CDK7 inhibitors THZ1,[3,6,7] we measured apoptosis by annexin V/propidium iodide (PI) staining (Figure S1D). Indeed, selective CDK7 inhibition by samuraciclib only induces a non-significant increase in the percentage of apoptotic cells, whereas THZ1 treatment causes apoptosis in most cells (Figure S1E). This was confirmed by the apoptotic marker cleaved caspase-3 in cells treated with THZ1, which is absent in samuraciclib-treated cell cultures (Figure S1F). This confirms previous observations showing that selective CDK7 inhibition is largely cytostatic rather than cytotoxic.

We next measured whether samuraciclib treatment inhibits cellular proliferation by analyzing EdU incorporation by flow cytometry. EdU is readily incorporated into DNA during S phase; therefore, EdU-positive cells represent the actively replicating cell population. We treated RPE1 cells for 48 h with samuraciclib or DMSO (vehicle control), then pulse labeled them with EdU for 1 h and analyzed EdU incorporation by flow cytometry. Treatment with samuraciclib leads to a striking decrease in the percentage of EdU-positive cells compared with control, with an almost complete loss of S-phase cells at higher concentrations (Figures 1A and 1B). Loss of the S-phase cell population, upon samuraciclib treatment, was confirmed by DNA content analysis

Figure 1. Samuraciclib inhibits proliferation of RPE1 cells by inducing cell-cycle arrest in G1

(A) RPE1 cells were treated with vehicle control or 120 nM of samuraciclib for 48 h. Cells were then incubated with EdU for 1 h before collection. Pseudocolored plots of flow cytometry data from one representative experiment. DNA content is plotted against EdU incorporation. Inset gate drawn to include EdU+ cells.

(B) RPE1 cells were treated with vehicle control or the indicated concentrations of samuraciclib for 48 h. Cells were then incubated with EdU for 1 h before collection. Quantification of the percentage of EdU+ cells (representative shown in A) within the population from three independent experiments. Statistical significance is represented by * and was determined using an unpaired two-tailed t test. Error bars show SD.

(C) RPE1 cells were treated with vehicle control or 120 nM of samuraciclib for 48 h. Flow cytometry data from one representative experiment. DNA content is plotted against cell count. Inset gates were drawn based on DNA content.

(D) RPE1 cells were treated with vehicle control or the indicated concentrations of samuraciclib for 48 h. Quantifications from three independent experiments (representative shown in C) showing the mean number of viable cells in each phase of the cell cycle.

(E) Schematic illustrating the experimental setup. RPE1 cells were labeled with EdU for 1 h. Unincorporated EdU was washed out of cells and the cells were treated with vehicle control or 120 nM of samuraciclib. Cells were collected at the indicated time points after drug addition and then analyzed using flow cytometry.

(F) Flow cytometry data from one representative experiment. DNA content is plotted against cell count. In red are all cells in the sample and overlaid in blue are the EdU+ cells.

(G) Quantifications from three independent experiments (representative shown in F) showing the percentage of EdU+ cells in the different phases of the cell cycle. Error bars show SD.

(H) RPE1-FUCCI cells were treated with vehicle control or 120 nM of samuraciclib and imaged for 48 h. Representative tracks of 100 cells, at final time point, are shown for samuraciclib treatment and 50 for vehicle control.

(I) Quantification of data of >200 cells tracked to determine cell-cycle progression during 48 h of samuraciclib treatment. State refers to cell-cycle state at final time point based on tracking of FUCCI reporter. G1, red; M.b., mitotic bypass, where cells turn red without going through mitosis; G2, green; M.c., mitotic catastrophe, where cells die after going through mitosis; and G1/S, yellow.

via PI staining and flow cytometry (Figures 1C, 1D, and S1G). This analysis, which shows percentage of cells in the G1, S, and G2 phases of the cell cycle, indicates that selective CDK7 inhibition predominantly arrests cells in the G1 phase of the cell cycle, with a reduced G2 population.

Because CDK7 is required for the activity of all mitotic CDKs,[10,11] we wanted to establish if samuraciclib treatment blocks cells at the G1-to-S transition or also slows down cell-cycle progression via a G2 arrest. To assess the G2-M and G1-S transitions during samuraciclib treatment, we decided to follow cell-cycle progression of the S-phase population upon samuraciclib treatment. The S-phase population of RPE1 cells was pulse labeled with EdU for 1 h prior to drug treatment. Unincorporated EdU was washed away before samuraciclib or vehicle was added, and EdU-positive cells, representing the S-phase population when treatment started, were analyzed at the indicated time points by flow cytometry (see schematic in Figure 1E) for up to 24 h. This allowed the analysis of the progression of the S-phase cell population, labeled at time point 0, through the cell cycle during samuraciclib treatment (Figures 1F and 1G). In control cells, we observed that the population of cells labeled in S phase completed an entire cell cycle, reentering S phase at 24 h. However, although samuraciclib-treated cells progressed normally through the G2 and M phases, they collectively arrested with a G1 DNA content (Figure 1G). Although CDK7 is required to establish the active state of all mitotic CDKs, the G1-specific arrest is the likely result of CDK7 also being required for maintaining CDK4 and CDK6 activity, as is not the case for CDK1 and CDK2.[12]

These results were confirmed by western blot analysis of protein markers associated with a G1 specific arrest (Figure S1H). We observed a decrease in levels of phosphorylated Rb, which coincided with an increase in levels of the CDK inhibitor $p21^{CIP1}$, both well-known markers of cell-cycle arrest in G1[13] (Figure S1H). This suggests that samuraciclib-treated cells can progress through the cell cycle but are unable to enter a new cell cycle. Importantly, the levels of the DNA damage markers, CDK4/6 inhibitor $p16^{INK4a}$, (Figure S1I) and the ataxia telangiectasia mutated (ATM) targets, Chk2 phosphorylated at Thr68 (Figure S1J) and γH2AX (Figures S1J–S1M) do not increase, suggesting that samuraciclib treatment does not activate the DNA damage response, as supported by previous observations.[3] These data indicate that samuraciclib treatment is unlikely to induce DNA damage or depends on the DNA damage response to cause the G1 arrest.

To complement our snapshot analysis, we carried out live-cell imaging using RPE1-FUCCI cells, which allows monitoring the progression of single cells through the cell cycle[14] in control conditions and during a samuraciclib-induced arrest (Figures 1H and 1I). These data show that in control conditions, within the 48-h time frame, most of the cells progress through the cell cycle at least twice (Figure 1H). However, consistent with our observations, during a 48-h samuraciclib treatment, the vast majority of cells end up in a G1 state (Figure 1H). Only a limited number of samuraciclib-treated cells enter a new cell cycle within the 48-h time frame, which we define as going from S-G2-M (green),to M/G1 (blank), to G1 (red) and then entering a new cell cycle (from red, to yellow, to green). After 48 h of samuraciclib treatment, the FUCCI reporter red cells include a proportion of G2 cells that underwent mitotic bypass where G2, green cells, skip the M/G1, blank stage, and enter a G1, red state. However, none to very few cells undergo mitotic catastrophe (Figure 1I). This is in line with our observations that samuraciclib treatment does not cause cell death nor activates the DNA damage response. Overall, these data establish that samuraciclib mainly inhibits cell proliferation via inducing a G1 arrest, which is independent of DNA damage signaling and cell death.

Samuraciclib induces a permanent cell-cycle exit via senescence

We next investigated whether samuraciclib induces a cell-cycle arrest or an irreversible cell-cycle exit. For this purpose, we tested if cells could proliferate after samuraciclib treatment. RPE1 cells were treated with samuraciclib for 2 days, after which the drug, which is not covalently bound, was washed out and cells were allowed to grow for an additional 2 or 5 days in culture (see schematic in Figure S2A). Cell proliferation was assayed by measuring EdU incorporation via flow cytometry (Figure S2B). Strikingly, the inhibition of cell proliferation observed upon 2 days of samuraciclib treatment persists for up to 5 days after the drug wash-out (Figure 2A). This suggests that the inhibition of cell proliferation induced by samuraciclib is the result of a permanent cell-cycle exit.

An irreversible exit from the cell cycle is the hallmark of a senescent state.[15] To further assess if samuraciclib induces a senescent state, we investigated additional markers of senescence. A widely used marker of senescence is an increase in senescence-associated (SA) β-galactosidase activity.[16,17] Treatment with samuraciclib for 4 days results in a clear increase in the number of cells showing a blue staining in their cytoplasm, indicative of SA β-galactosidase activity, compared with control cells (Figure 2B). A more quantitative assessment of SA β-galactosidase activity, using flow cytometry (Figure 2C), indicates a significant increase in SA β-galactosidase activity over time in samuraciclib-treated cells compared with control cells (Figure 2D). In addition, we observe a striking increase in median cell volume, measured by Coulter counter, in samuraciclib-treated compared with control cells (Figures 2E and 2F), which is another phenotypic characteristic of senescent cells.[15] Finally, in addition to an increase in $p21^{CIP1}$ levels (Figure S1H), we also observe a decrease in Lamin B1 levels (Figure 2G), both indicators of a senescent state.[18,19] Together, these data indicate that selective inhibition of CDK7 induces a senescent phenotype.

Sensitivity to samuraciclib depends on active mTOR signaling

To gain insight into the mechanisms via which CDK7 inhibition induces senescence, we carried out a genome-wide CRISPR KO chemogenetic screen. The screen was performed in NALM-6 cells, a B cell precursor leukemia cell line, which grow in suspension making them particularly suited for this approach. In addition, their lower sensitivity to samuraciclib allows identification of both positive and negative interactors. A pooled custom extended-KO (EKO) library of 278,754 different single-guide RNAs (sgRNAs), which targeted 19,084 RefSeq genes, 20,852 unique alternative exons, and 3,872 hypothetical genes, was

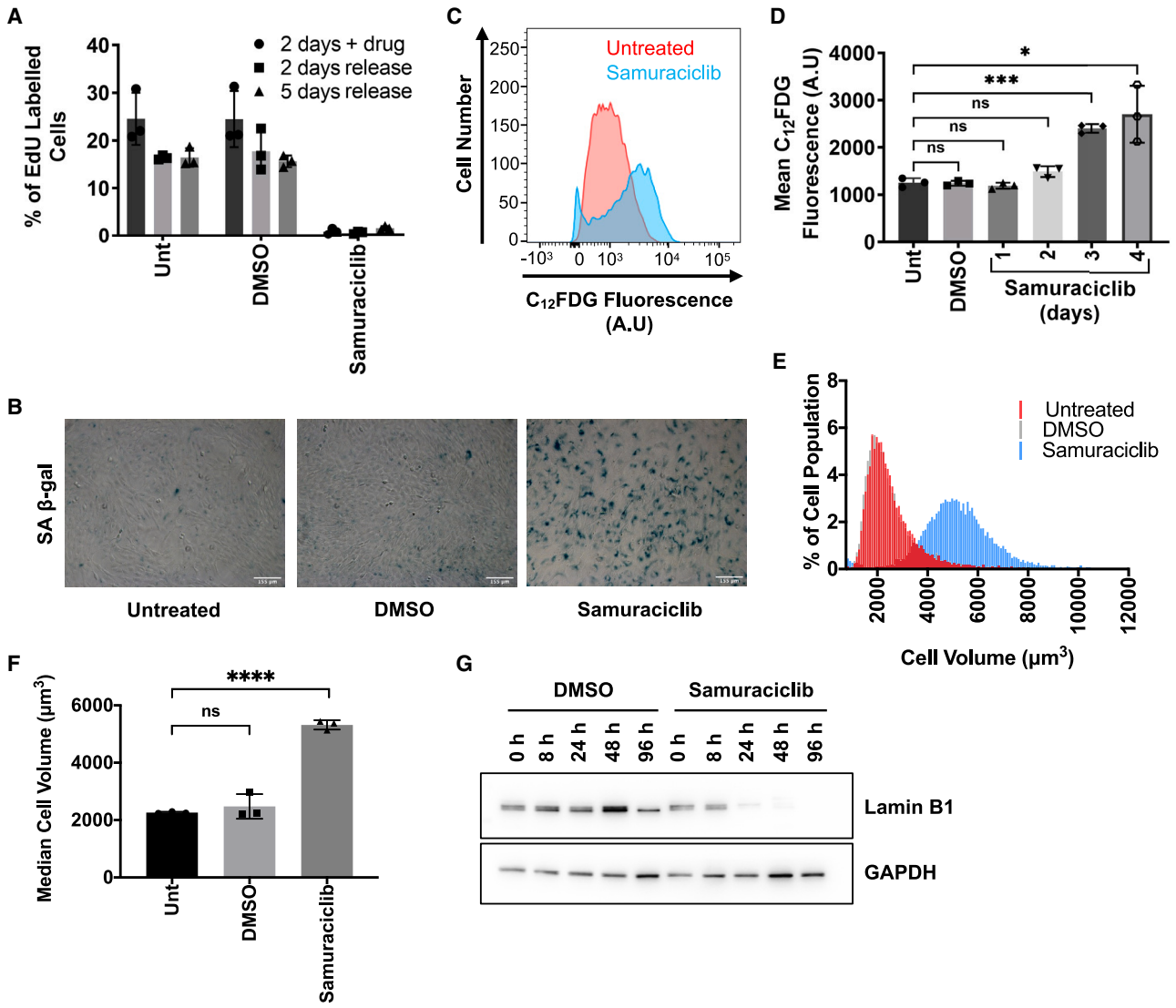

Figure 2. CDK7i induces a senescent phenotype in RPE1 cells

(A) RPE1 cells were treated with vehicle control or 120 nM of samuraciclib for 48 h. After 48 h some cells were labeled with EdU for 1 h and then harvested. Other cells were washed thoroughly with PBS and given fresh culture media to remove samuraciclib from the cells. These cells were then allowed to grow in culture for another 2 or 5 days, before undergoing EdU labeling and harvesting. Quantification of the percentage of EdU+ cells within the population from three independent experiments. Error bars show SD.

(B) Representative images of detection of SA β-gal activity in RPE1 cells with the chromogenic β-gal substrate, X-gal in untreated cells and cells treated with vehicle control or 120 nM of samuraciclib for 4 days. Scale bar represents 155 μm.

(C) Flow cytometry data from one representative experiment, detecting SA β-gal activity with the fluorescent β-gal substrate, 5-dodecanoylaminofluorescein di-β-D-galactopyranoside (C_{12}FDG) in untreated cells and cells treated with 120 nM of samuraciclib for 4 days. C_{12}FDG fluorescence is plotted against cell count.

(D) Quantification of the mean C_{12}FDG fluorescence within populations of cells that were untreated or treated with vehicle control or 120 nM of samuraciclib for up to 4 days from three independent experiments (representative shown in C). Statistical significance is represented by * and was determined using an unpaired two-tailed t test. Error bars show SD.

(E) Coulter counter data from one representative experiment, with RPE1 cells treated with vehicle control or 120 nM samuraciclib for 48 h. Percentage of cell population is plotted against various bins containing cells with different volumes in μm^3.

(F) Coulter counter data quantification of the median cell volume within the population from three independent experiments. Statistical significance is represented by * and was determined using an unpaired two-tailed t test. Error bars show SD.

(G) Western blot analysis from one experiment of whole-cell extract collected from RPE1 cells at the indicated time points after treatment with vehicle control or 120 nM of samuraciclib. GAPDH: loading control.

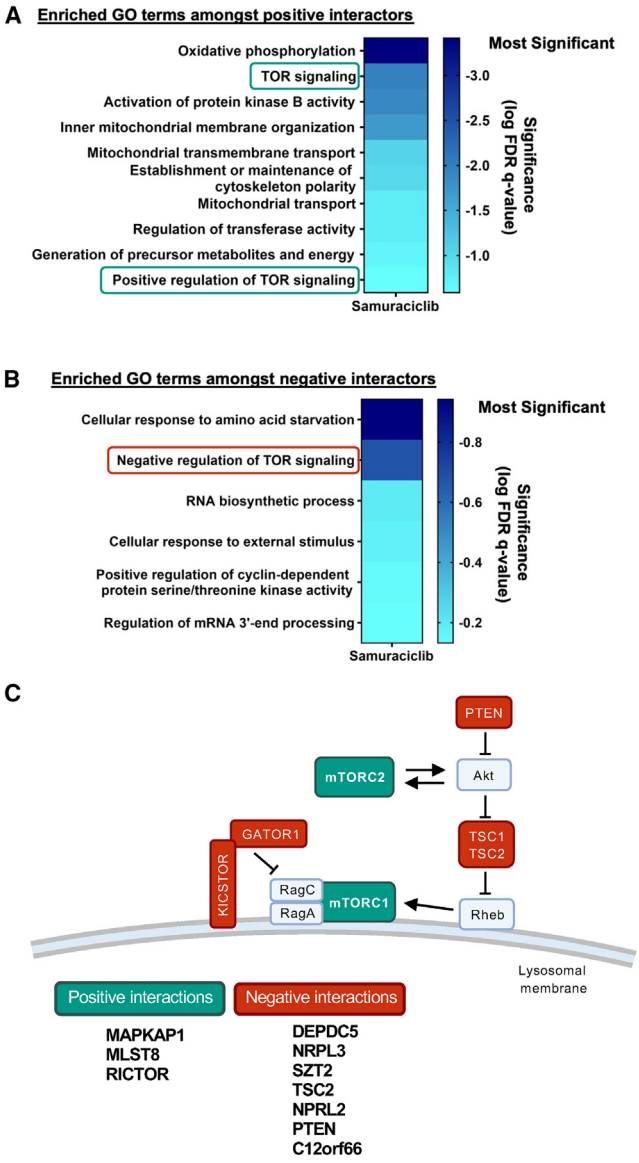

Figure 3. A genome-wide CRISPR knockout screen indicates that mTOR signaling is central to CDK7i-induced senescence

(A) Heatmap representation of the most enriched GO terms among the top 20 positive interactors of samuraciclib, as determined using the GOrilla tool[21,22] and processing by REVIGO.[23] They are color coded according to the scale on the right, which represents the log (false discovery rate [FDR] q-value). The GO terms closer to the dark blue end of the scale have the most statistically significant FDR q-value, and the GO terms closer to the light blue end of the scale have the least statistically significant FDR q-value. Positive mTOR GO terms are highlighted by green boxes.

(B) Heatmap representation of the most enriched GO terms among the top 20 negative interactors of samuraciclib, as determined using the GOrilla tool[21,22] and processing by REVIGO.[23] Color-coding on the right represents the log (FDR q-value). The GO terms closer to the dark blue end of the scale have the most statistically significant FDR q-value and the GO terms closer to the light blue end of the scale have the least statistically significant FDR q-value. Negative mTOR GO terms are highlighted by red box.

(C) Simplified schematic of the mTOR signaling pathway. The boxes and listed genes indicate some of the components of the signaling pathway that were among the top 100 positive interactors of samuraciclib (green boxes) and the top 100 negative interactors of samuraciclib (red boxes), as identified by the genome-wide CRISPR knockout chemogenetic screen. Gene names of all GO term included mTOR hits are listed below.

used.[20] We confirmed that samuraciclib is also able to reduce proliferation and cell-cycle progression in this cell line (Figures S3A–S3D).

Positive interactors (relative enrichment of sgRNAs) represent genes required for samuraciclib sensitivity and the induction of a senescent state, and their inactivation are possible resistance mechanisms (Figure 3A). Negative interactors (relative depletion of sgRNAs) represent proteins and processes involved in preventing samuraciclib-induced senescence, whose inactivation would increase samuraciclib sensitivity and potentially improve the outcome of individual patients (Figure 3B). The robust analytics and normalization for knockout screens (RANKS) tool[20] was used to identify genes that may have positive or negative interactions with samuraciclib based on the relative abundance of each sgRNA in samuraciclib-treated cells compared with a control cell population. We carried out gene ontology (GO) enrichment analysis on the genes that were identified as the top 20 positive and negative interactors with samuraciclib (Figures 3A and 3B). For positive interactors, "TOR signaling" and "positive regulation of TOR signaling" were among the most enriched GO terms (Figure 3A). Strikingly, for negative interactors, "negative regulation of TOR signaling" was among the most enriched GO terms (Figure 3B). In addition, the absence of DNA damage response, apoptosis, and cell-cycle regulator signatures, which we consistently find in our anti-cancer drug chemogenetic screens, is striking and confirms the absence of the DNA damage markers (Figures S1J–S1M) after samuraciclib treatment. The overall lack of cell-cycle regulators suggests that CDK7 inhibitors can trigger cell-cycle exit independent of the canonical cell-cycle exit (p16/ATM-p53) and/or cell-cycle entry pathways (Ras-Raf-Mek-Erk-c-Myc-CyclinD/CyclinE-Rb-E2F). This is distinctly different from inhibitors that selectively target CDK4/6[1] and suggests that CDK7 inhibition could potentially benefit a wider range of patients. Overall, our genome-wide CRISPR KO chemogenetic screen indicates that active mTOR signaling is important for sensitivity to selective CDK7 inhibition (Figure 3C).

Samuraciclib-induced senescence depends on mTOR signaling

Our screen data suggest that active mTOR signaling is important for the induction of samuraciclib-induced senescence. By extension, a reduction of mTOR signaling would decrease the sensitivity of cells to samuraciclib treatment. To test this, we used Torin1, an ATP-competitive mTOR inhibitor, to inhibit the mTOR signaling pathway. Phosphorylation of S6 kinase at threonine residue 389 and phosphorylation of the 40S ribosomal subunit protein S6 at serine residues 235 and 236 are generally used to establish mTOR inhibition.[24,25] Using these markers, we show that in our system Torin1 treatment, either alone or combined with samuraciclib, effectively inhibits mTOR signaling (Figure S4A). We also confirm that samuraciclib treatment alone or in combination with Torin1 results in a loss of phosphorylation

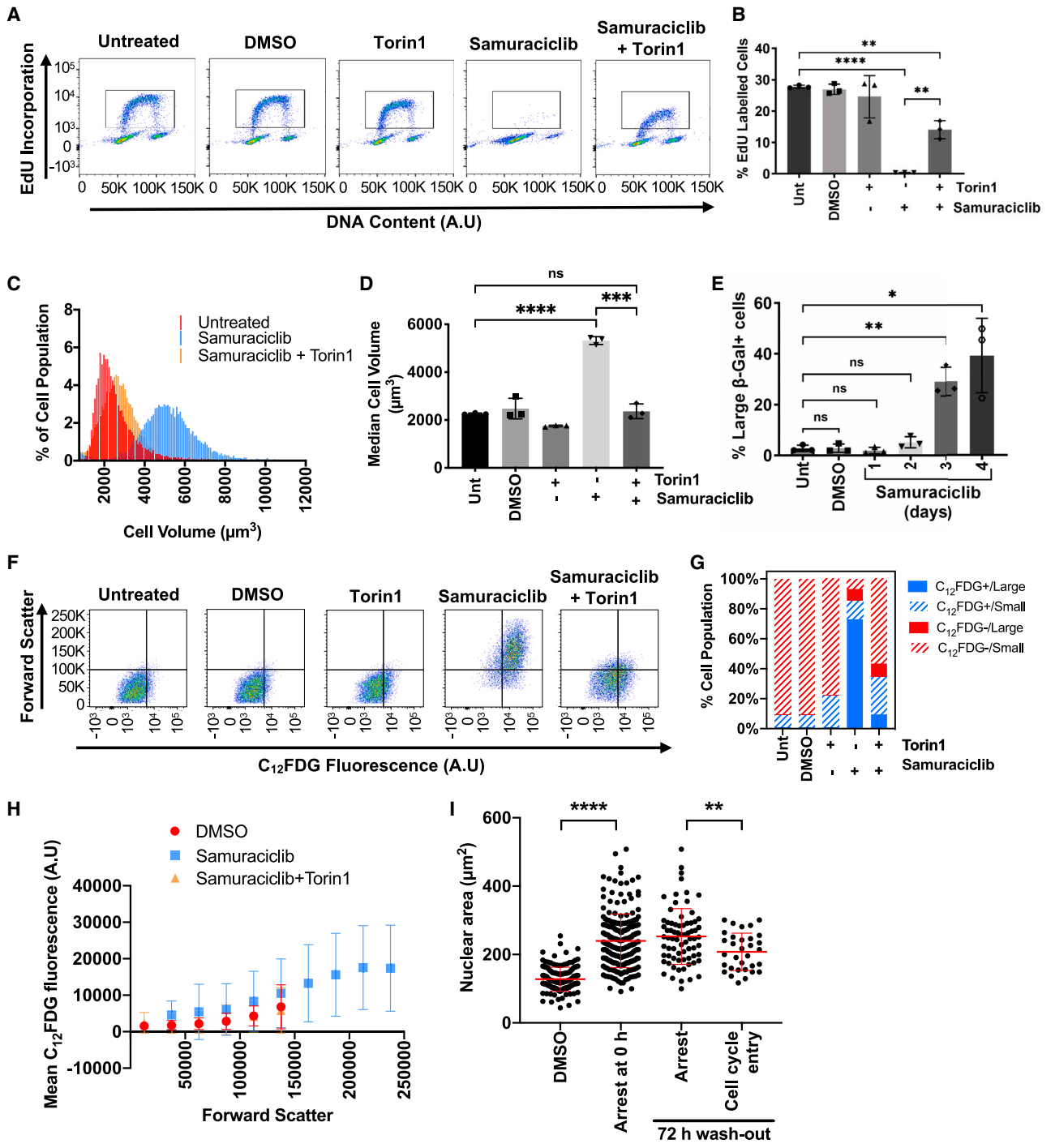

Figure 4. CDK7i-induced senescence is dependent upon active growth signaling in RPE1 cells

(A) RPE1 cells were treated with vehicle control, 25 nM of Torin1 alone, 120 nM of samuraciclib alone, or 120 nM of samuraciclib and 25 nM of Torin1 for 48 h. Cells were then incubated with EdU for 1 h before collection. Pseudocolored plots of flow cytometry data from one representative experiment. DNA content is plotted against EdU incorporation. Inset gate drawn to include EdU+ cells.

(B) Quantification of the percentage of EdU+ cells within the population from three independent experiments (representative shown in A). Statistical significance is represented by * and was determined using an unpaired two-tailed t test. Error bars show SD.

(C) Coulter counter data from one representative experiment, with RPE1 cells treated with vehicle control, 25 nM of Torin1 alone, 120 nM of samuraciclib alone, or 120 nM of samuraciclib and 25 nM of Torin1 for 48 h. Percentage of cell population is plotted against various bins containing cells with different volumes in μm^3.

(legend continued on next page)

of CDK1 (pThr161) and RNA Pol II (pSer5), demonstrating inhibition of CDK7 activity (Figure S4A). Interestingly, combined treatment results in a marked reduction of samuraciclib-induced $p21^{CIP1}$ accumulation and an apparent increase in Rb phosphorylation (pSer807-811) indicative of a rescue in proliferation (Figure S4A). To investigate this further, we assessed the effect of combined treatment on cellular proliferation by measuring EdU incorporation (Figure 4A). Combining 48-h samuraciclib and Torin1 treatments significantly increased the percentage of proliferating cells compared with samuraciclib alone, whereas Torin1 alone shows no effect compared with control (Figure 4B). Correspondingly, combined treatment of samuraciclib and Torin1 leads to a decrease in the percentage of cells in G1 compared with samuraciclib treatment alone (Figures S4C and S4D). These data suggest that active mTOR signaling is required for the G1 cell-cycle arrest induced by samuraciclib treatment.

To establish if active mTOR signaling is important for the samuraciclib-induced senescent phenotype, we assessed the effect of combined treatment of samuraciclib and Torin1 on a selection of the phenotypic characteristics of senescence previously observed upon samuraciclib treatment alone. Combining samuraciclib and Torin1 decreased SA β-galactosidase activity compared with samuraciclib treatment alone (Figures S4E and S4F) and led to a significant decrease in cell volume, compared with samuraciclib alone (Figures 4C and 4D). In addition, combined samuraciclib and Torin1 treatment also prevents an increase in $p21^{CIP1}$ levels and a decrease in Lamin B1 levels (Figures S4A and S4B). Altogether these data suggest that inhibition of mTOR activity impairs the ability of samuraciclib to induce a senescent phenotype in RPE1 cells.

mTOR-dependent cellular growth promotes increased cell size and samuraciclib-induced senescence

The mTOR signaling pathway is known to be a major regulator of cell growth.[26] It has been reported that continued growth, driven by signaling pathways, such as mTOR, during cell-cycle arrest can convert a reversible arrest to irreversible senescence.[27–29] We tested if mTOR-dependent continued cellular growth, and consequent increased cell size, is an important factor for samuraciclib-induced senescence. We first assessed if an increase in cell size, as a proxy for cellular growth, upon samuraciclib treatment correlates with SA β-galactosidase activity, a marker of senescence. We measured SA β-galactosidase activity using flow cytometry as in Figure S4E and plotted it against forward scatter (FSC), which can be used as a proxy of cell size.[30] We selected large cells based on FSC and compared SA β-galactosidase activity of this population between control and samuraciclib treatment at various time points (Figures S4G and S4H). We observed that there was an increase in the percentage of RPE1 cells that were large and had increased SA β-galactosidase activity with samuraciclib treatment compared with control (Figure 4E). To test if this increase in cell size and SA β-galactosidase activity required mTOR signaling, we treated the cells with both samuraciclib and Torin1 (Figures 4F and 4G). Inhibition of mTOR signaling decreased the percentage of large cells with increased SA β-galactosidase activity compared with samuraciclib alone, suggesting that increased SA β-galactosidase activity relies, in part, upon active mTOR signaling. A more detailed analysis of binned cell populations based on FSC clearly shows the positive correlation between cell size and SA β-galactosidase activity, a proxy for senescence (Figure 4H). Altogether these data suggest that an mTOR-dependent increase in cell size correlates with the ability of samuraciclib to induce senescence and therefore sensitivity to CDK7 inhibition.

To further investigate the relationship between cell size and a permanent samuraciclib-induced cell-cycle arrest, we carried out live-cell imaging, using RPE1-FUCCI cells (Figure 4I). We determined nuclear size, as a proxy for cell size, of FUCCI red cells in proliferating culture (DMSO) and samuraciclib arrest (72-h treatment = arrest at 0 h) culture. This shows that cells significantly increase in size during the arrest. We then monitored which cells enter the cell cycle within a 72-h time frame after wash-out. These data indicate that smaller cells are more likely to return to a proliferative state after samuraciclib wash-out than bigger cells. This suggests that cell size, which depends on growth rate, is an important indicator of a permanent arrest, i.e., samuraciclib sensitivity.

Samuraciclib sensitivity positively correlates with mTOR-dependent growth signaling in breast cancer cell lines

Our data show that a samuraciclib-induced senescent state depends on mTOR activity in non-transformed RPE1 cells. These data indicate that mTOR-dependent cellular growth plays an important role in samuraciclib sensitivity, likely by driving an increase in cell size to induce senescence during a G1 arrest. With increased growth signaling being a common feature of cancer cells, this could explain the increased sensitivity to CDK7

(D) Quantification of the median cell volume within the population from three independent experiments (representative shown in E). Statistical significance is represented by * and was determined using an unpaired two-tailed t test. Error bars show SD.
(E) Quantification of the percentage of large cells that are C_{12}FDG+ from three independent experiments. Statistical significance is represented by * and was determined using an unpaired two-tailed t test. Error bars show SD.
(F) RPE1 cells were treated with vehicle control, 25 nM of Torin1 alone, 120 nM of samuraciclib alone, or 120 nM of samuraciclib and 25 nM of Torin1 for 4 days. Pseudocolored plots of flow cytometry data from one experiment. C_{12}FDG fluorescence is plotted against forward scatter, a measure of cell size. Quadrant drawn to distinguish between small, C_{12}FDG− cells, small, C_{12}FDG+ cells, large, C_{12}FDG− cells and large, C_{12}FDG+ cells.
(G) Quantification of data shown in (F) indicating the percentage of small, C_{12}FDG− cells, small, C_{12}FDG+ cells, large, C_{12}FDG− cells and large, C_{12}FDG+ cells.
(H) Data from (F) binned by cell size based on forward scatter (FSC) and divided into ten bins. Mean C_{12}FDG fluorescence is measured for each cell size bin. Error bars show SD.
(I) RPE1-FUCCI cells were treated with vehicle control or 120 nM of samuraciclib for 72 h. After 72 h, cells were washed with PBS five times to remove samuraciclib from the cells, and fresh media was added, after which live-cell imaging was started for 72 h. Nuclear area was measured for red cells at the first time point (0 h). 105 cells were tracked after samuraciclib wash-out to determine cells that remain arrested and cells that enter the cell cycle. Statistical significance is represented by * and was determined using an unpaired two-tailed t test. Error bars show SD.

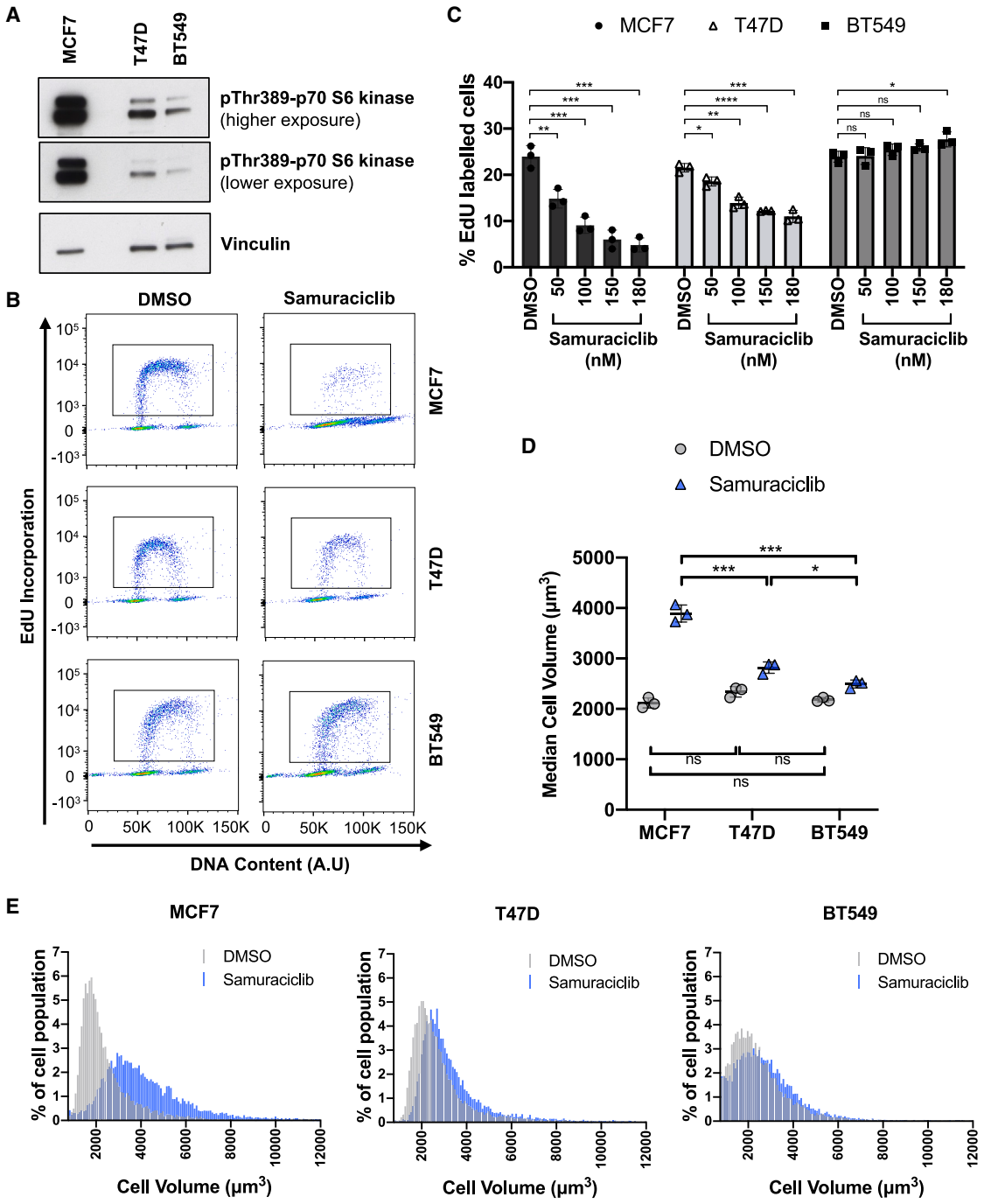

Figure 5. CDK7i sensitivity positively correlates with mTOR-dependent growth signaling in breast cancer cell lines

(A) Western blot analysis from one representative experiment of whole-cell extract collected from MCF7, T47D, and BT549 cells. Vinculin: loading control.

(B) MCF7, T47D, and BT549 cells were treated with vehicle control or 180 nM of samuraciclib for 4 days. Cells were then incubated with EdU for 1 h before collection. Pseudocolored plots of flow cytometry data from one representative experiment. DNA content is plotted against EdU incorporation. Inset gate drawn to include EdU+ cells.

(C) MCF7, T47D, and BT549 cells were treated with vehicle control or the indicated concentrations of samuraciclib for 4 days. Cells were then incubated with EdU for 1 h before collection. Quantification of the percentage of EdU+ cells (representative shown in B) within the population from three independent experiments. Statistical significance is represented by * and was determined using an unpaired two-tailed t test. Error bars show SD.

(legend continued on next page)

inhibition observed in many cancers. To test this, we investigated if samuraciclib sensitivity correlates with mTOR-dependent growth signaling in breast cancer cells, previously shown to be sensitive to samuraciclib.[3] Three cell lines were selected with different growth-inducing mutations upstream of mTOR, MCF7 (*PIK3CA*: E545K), T47D (*PIK3CA*: H1047R), and BT549 (PTEN-deficient).[31,32] mTOR pathway activity was assessed by establishing Thr389 phosphorylation of the mTOR target 70-kDa ribosomal protein S6 kinase (pThr389-p70S6K), known to regulate cell growth by inducing protein synthesis components (Figure 5A). Our data indicate that pThr389-p70S6K is highest in MCF7 cells with markedly lower levels in T47D and BT549 cells. T47D cells, in turn, show slight but consistently higher levels than BT549 cells (Figures 5A, S5A, and S5B). Next, we tested their sensitivity to samuraciclib by assessing cellular proliferation by measuring EdU incorporation (Figures 5B and 5C). This shows a marked decrease in proliferating cells in MCF7 cells upon samuraciclib treatment, with a smaller effect on cell proliferation in T47D cells and no effect upon cell proliferation in BT549. The effect of samuraciclib upon cellular proliferation correlates with the level of mTOR-dependent growth signaling in these cell lines. Furthermore, the correlation between sensitivity and growth signaling is in line with the samuraciclib-induced increase in cell size observed in these cell lines (Figures 5D and 5E). These data indicate that samuraciclib sensitivity positively correlates with mTOR-dependent cellular growth signaling and an increase in cell size during treatment.

Samuraciclib sensitivity correlates with induction of senescence in MCF7 cells

The high levels of mTOR signaling observed in MCF7 cells correlates with high sensitivity to samuraciclib and a more pronounced increase in cell size during treatment compared with the other breast cancer cell lines. Senescence bypass is thought to be an important step in tumorigenesis and a number of genes encoding proteins integral to senescence induction are commonly mutated in cancer.[33] We therefore wanted to confirm that the samuraciclib-induced cell-cycle arrest in MCF7 cells was because of senescence induction, as in non-transformed RPE1 cells. Treatment with samuraciclib led to a clear decrease in phosphorylated Rb and Lamin B1 levels and an increase in $p21^{CIP1}$ levels and SA β-galactosidase activity in MCF7 cells compared with control (Figures S5C–S5F). Altogether, these data indicate that inhibition of CDK7 induces a senescent phenotype in tumor-derived MCF7 cells.

Growth-stimulating mutation in MCF7 cells promotes samuraciclib sensitivity

Our data indicate that cellular growth may be one of the key drivers that determine CDK7i sensitivity. Based on this, cancer-associated mutations that drive cellular growth independently of proliferative signals could be at the basis of the increased sensitivity of cancer cells to CDK7i, such as samuraciclib. MCF7 cells harbor a mutation in *PIK3CA* (E545K), the gene encoding the catalytic subunit of phosphatidylinositol 3-kinase (PI3K). This mutation has been shown to hyperactivate the PI3K/Akt/mTOR pathway, driving cell growth.[34] The *PIK3CA* gene has been shown to be mutated in 20%–50% of all breast cancers, and the E545K mutation occurs at one of three "hotspots" frequently mutated in breast cancer.[35]

To examine the interaction between samuraciclib and this clinically relevant growth-promoting mutation, we utilized a pair of isogenic MCF7 cell lines, one with the E545K *PIK3CA* mutation ($PIK3CA^{mut}$) and one where the *PIK3CA* gene has been reverted back to the wild-type sequence ($PIK3CA^{wt}$).[36] We confirm that there is increased activation of the PI3K/Akt/mTOR pathway in the $PIK3CA^{mut}$ cells compared with the $PIK3CA^{wt}$ (Figures 6A and 6B), in line with previous data, indicating that the E545K mutation induces hyperactivation of this signaling pathway. We also established the sensitivity of the parental MCF7 $PIK3CA^{mut}$ cell line of this isogenic pair (Figures S6A and S6B).

To compare the sensitivity of the $PIK3CA^{mut}$ and $PIK3CA^{wt}$ cells, we treated them with samuraciclib for 30 days with various drug concentrations, and cell numbers were assessed using an IncuCyte (Figure 6C). These data show a marked decrease in sensitivity of the $PIK3CA^{wt}$ cells, when compared with the $PIK3CA^{mut}$ cells. The number of $PIK3CA^{mut}$ cells was very low throughout the 30 days for all concentrations, indicating that samuraciclib strongly inhibited the proliferation of these cells (Figures 6D and S6C). Samuraciclib also inhibited the proliferation of $PIK3CA^{wt}$ cells, when compared with untreated control cells, but these cells were less sensitive to samuraciclib treatment than the $PIK3CA^{mut}$ cells and continued to proliferate, particularly at lower concentrations (Figures 6D and S6C).

The difference in sensitivity correlates with a significantly larger median cell volume increase of $PIK3CA^{mut}$ cells compared with the $PIK3CA^{wt}$ cells at lower drug concentrations (Figures 6E, S6D, and S6E), indicating that increased cellular growth correlates with increased cell size and sensitivity to samuraciclib. These data suggest that cancer-associated mutations that promote cellular growth may be at the basis of cancer cell sensitivity to CDK7 inhibition.

DISCUSSION

In this study, we investigated the mechanism by which CDK7 inhibition arrests cellular proliferation to establish the key fundamental cellular processes that determine sensitivity to CDK7 inhibitors. Insight into this will guide the use of CDK inhibitors and promote the future clinical use of CDK7, and other mitotic CDK, inhibitors. Samuraciclib was used in our study because of its high selectivity to inhibit CDK7 and its non-covalent

(D) MCF7, T47D, and BT549 cells were treated with vehicle control or 180 nM of samuraciclib for 4 days. Quantification of the median cell volume within the population from three independent experiments (representative shown in E). Statistical significance is represented by * and was determined using an unpaired two-tailed t test. Error bars show SD.

(E) Coulter counter data from one representative experiment, with MCF7, T47D, and BT549 cells treated with vehicle control or 180 nM samuraciclib for 4 days. Percentage of cell population is plotted against various bins containing cells with different volumes in μm^3.

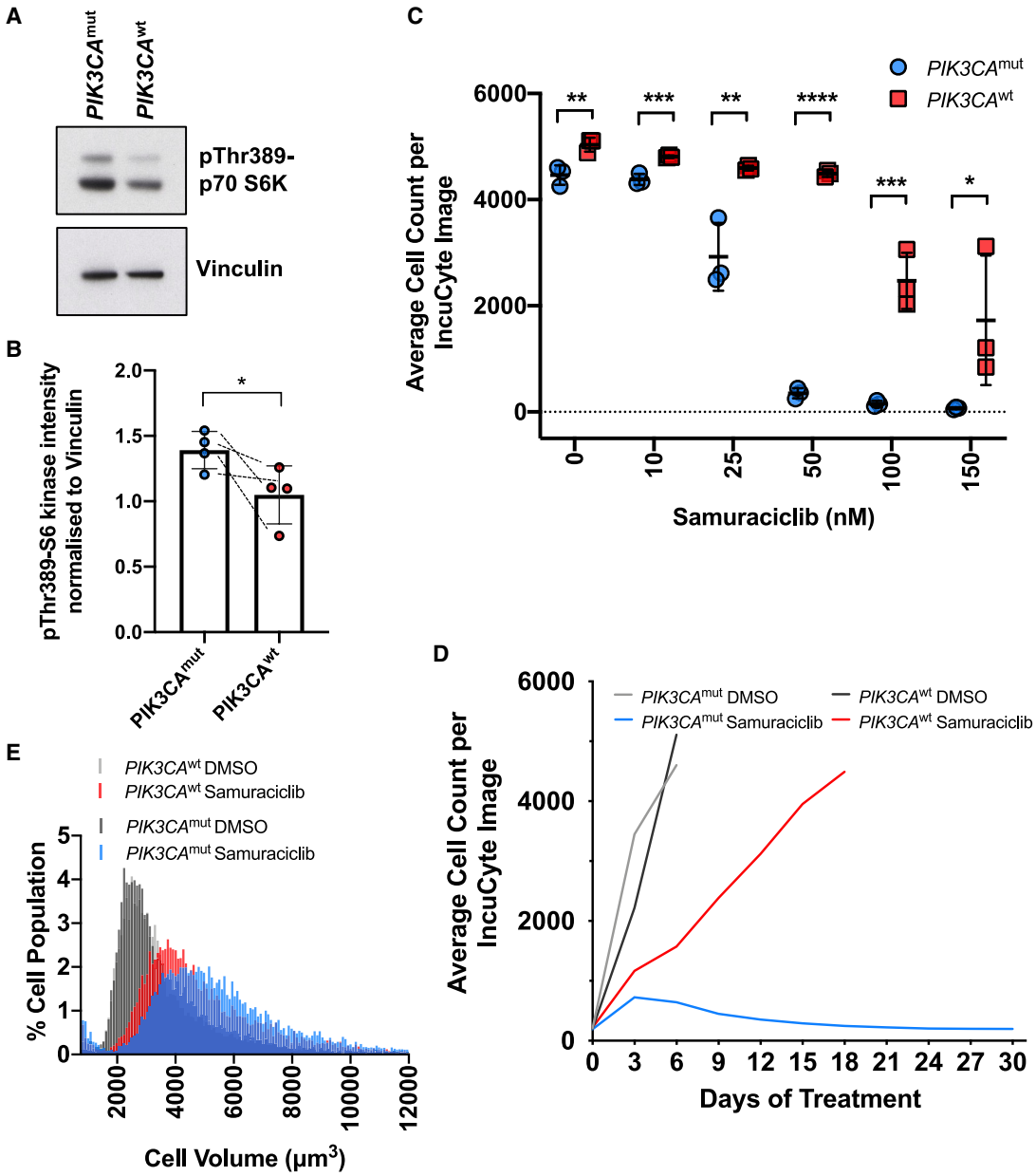

Figure 6. Growth-stimulating mutation in MCF7 cells promotes samuraciclib sensitivity

(A) Western blot analysis from one representative experiment of whole-cell extract collected from *PIK3CA*^{mut} and *PIK3CA*^{wt} MCF7 cells. Vinculin: loading control.

(B) Quantification of levels of p70 S6 kinase phosphorylated at residue Thr389 normalized to Vinculin as detected by western blots of whole-cell extracts from *PIK3CA*^{mut} and *PIK3CA*^{wt} MCF7 cells from four independent experiments. Statistical significance is represented by * and was determined using an unpaired two-tailed t test. Error bars show SD.

(C) *PIK3CA*^{mut} and *PIK3CA*^{wt} MCF7 cells were treated with vehicle control or the indicated concentration of samuraciclib for 30 days. Cell numbers were assessed by IncuCyte every 3 days. Cell growth is plotted until day 30 or until cells reached confluency. Quantification of average cell numbers after 18 days of treatment from three independent experiment. Statistical significance is represented by * and was determined using an FDR corrected unpaired t test.

(D) *PIK3CA*^{mut} and *PIK3CA*^{wt} MCF7 cells were treated with vehicle control or 50 nM of samuraciclib for 30 days. Cell numbers were assessed by IncuCyte every 3 days. Cell growth is plotted until day 30 or until cells reached confluency. Cell growth curves from a single representative experiment.

(E) Coulter counter data from one representative experiment, with *PIK3CA*^{mut} and *PIK3CA*^{wt} MCF7 cells treated with vehicle control or 50 nM of samuraciclib for 4 days. Percentage of cell population is plotted against various bins containing cells with different volumes in μm^3.

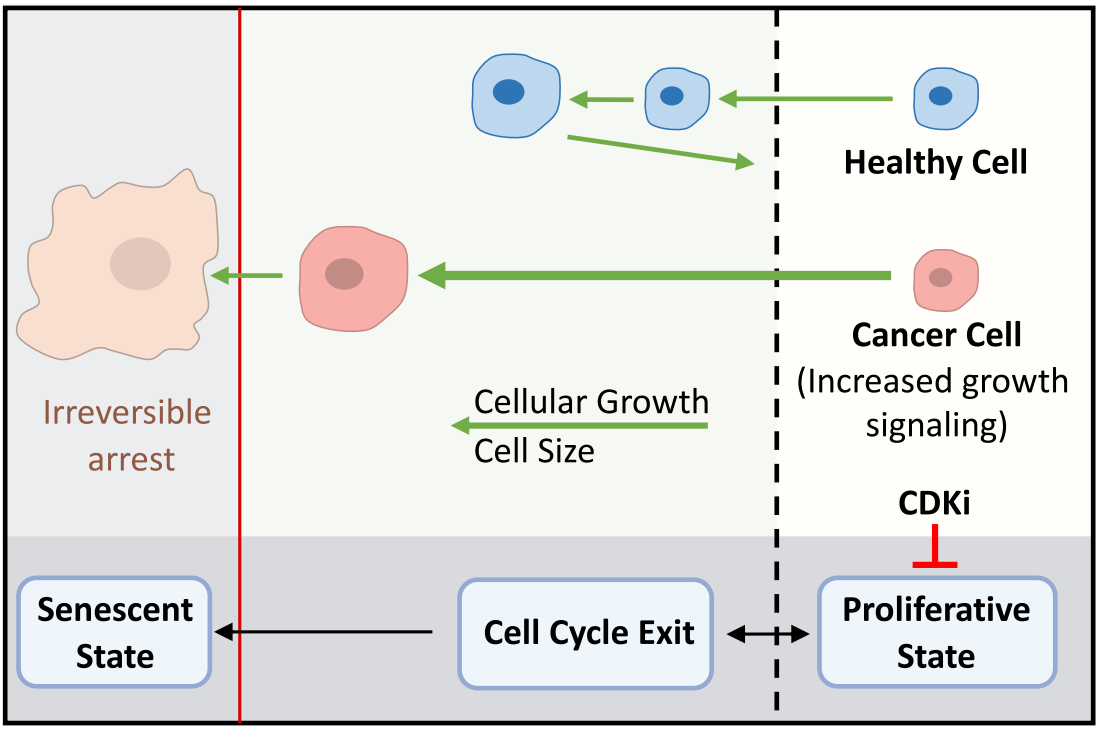

Figure 7. A model for how active growth signaling promotes senescence and cancer cell sensitivity to CDK7 inhibition

Schematic illustration of how an increase in cell size beyond a particular cell volume can cause uncoupling of protein synthesis with cell size resulting in a decrease in cytoplasm density, termed cytoplasmic dilution, which is thought to be the basis of irreversible cell-cycle arrest. As indicated by our data, active cellular growth, and the resulting increase in cell size (green arrow) during mitotic CDK inhibition (red T-junction), are important drivers of the senescent state. In the context of cancer biology and its treatment, oncogenic signals that stimulate cellular growth increase sensitivity to CDK inhibitors.

binding, which allowed investigation of release and recovery from CDK7 inhibition.

Our data indicate that CDK7 inhibition induces cell-cycle exit through senescence in the G1 phase of the cell cycle. Our genome-wide CRISPR KO chemogenetic screen indicates active cellular growth as a key fundamental cellular process that determines CDK7i sensitivity. Because growth-promoting mutations are present in many cancers, our data suggest that increased cellular growth is likely at the basis of why cancer cells are more sensitive to CDK7 inhibition than normally growing cells. These findings are in line with a recent study investigating CDK4/6 inhibition sensitivity.[37] In addition, our screen identified additional pathways, affecting CDK7i sensitivity, involved in energy generation, phosphorylation, and RNA processes. Although many of these processes can be linked to cell growth, their role in CDK7i sensitivity warrant further investigation.

Strikingly, inhibiting mTOR signaling greatly impairs the action of samuraciclib, limiting cell size by reducing cellular growth, allowing cells to maintain, or return to, a proliferative state. This suggests that CDK7i and CDK4/6 inhibitors[37] should not be used in combination with growth inhibiting anti-cancer drugs because this would prevent a permanent cell-cycle exit. It also indicates that, counterintuitively, drugs that promote cellular growth when combined with anti-proliferating drugs could greatly induce permanent cell-cycle exit. In terms of patient stratification, it reveals that CDK7 inhibitors may be more effective in tumors with highly active growth signaling. These include cancers with mutations in the PI3K/Akt/mTOR signaling pathway, which is thought to be one of the most commonly disrupted pathways in cancer.[38]

Overall, our data show that larger cells tend to be more senescent than smaller cells and that reducing cell size, by inhibiting mTOR signaling, decreases the percentage of senescent cells. This supports a model where increasing cell size beyond a "point of no return" might represent a key driver for preventing proliferation and inducing a permanent cell-cycle exit (Figure 7). This is in line with work in yeast, which shows that an increase in cell volume beyond a particular point causes "cytoplasmic dilution" and permanent cell-cycle exit,[30] and also in hematopoietic stem cells *in vivo*, which shows that cellular enlargement during aging leads to cellular dysfunction.[39] Importantly, a recent study in mammalian cells shows that increasing cell size itself results in proteome changes that gradually approach those found in senescent cells.[40] This supports the hypothesis that cellular growth signaling, driving an increase in cell size per se, promotes senescence.[41] Interestingly, this work and two other recent studies, show that an increase in cell size in cells arrested in the cell cycle by a CDK4/6 inhibitor compromises a cells' ability to re-enter the cell cycle.[42,43] Together this indicates that increased growth signaling is an important determinant for the increased sensitivity of

cancer cells to CDK inhibitors that inhibit cellular proliferation through senescence induction (Figure 7). Testing this in *in vivo* models will increase the chances of successful CDK7i approval and guide CDK4/6i clinical use. More fundamentally, it will establish the potentially central role of cellular growth, in both cancer and healthy cells, in driving a permanent exit from the cell cycle.

Limitations of the study

Our work presents a strong case for the concept that active cellular growth is an important determinate of the response of cancer cells to CDK7 inhibitor-induced senescence. However, whether an increase in cell size is sufficient to cause a permanent arrest needs further analysis. Our data show a strong correlation between cell size and a permanent arrest, but there is no binary distinction, i.e., a clear threshold. This might indicate that cellular growth signaling drives a permanent arrest partially independent of cell size, but other options are possible. For example, higher stress levels (genotoxic, proteotoxic, osmotic, etc.) of individual cells might prevent some small cells from re-entering the cell cycle. Alternatively, or in addition, some large cells might stay longer in a G1 state, rather than exiting the cell cycle, which could allow them to reenter the cell cycle. Future work should focus on testing these options and other possibilities to establish the role of cell size in a permanent cell-cycle exit.

Although the current work is a mode of action study aimed at disease positioning (stratification) a better mechanistic understanding should be established in more clinically relevant environment, such as organoids or spheroids. In addition, the clinical relevance of our finding should be established using patient-derived xenograft models and on samples from clinical trials, which is particularly timely, considering the recent FDA fast tracking of the CDK7 inhibitor samuraciclib.

STAR★METHODS

Detailed methods are provided in the online version of this paper and include the following:

- KEY RESOURCES TABLE
- RESOURCE AVAILABILITY
  - Lead Contact
  - Materials availability
  - Data and code availability
- EXPERIMENTAL MODEL AND STUDY PARTICIPANT DETAILS
- METHOD DETAILS
  - Drug treatments
  - Cell proliferation and viability
  - Flow cytometry
  - Western blot
  - Immunofluorescence
  - Detection of senescence-associated β-galactosidase activity
  - Quantification of cell volume
  - Live-cell imaging and analysis
  - Genome-wide CRISPR knock-out chemogenetic screen
  - Next Generation Sequencing
- QUANTIFICATION AND STATISTICAL ANALYSIS

SUPPLEMENTAL INFORMATION

Supplemental information can be found online at https://doi.org/10.1016/j.molcel.2023.10.017.

ACKNOWLEDGMENTS

We would like to thank Killian O'Kane and Erben Ostler de Bruin for their help with the FUCCI reporter single cell tracking data presentation and Waratchaya Naksiang for advice and support. In addition, we would like to thank Buzz Baum and Stephen Elledge for sharing cell lines and the LMCB Light Microscopy core facility for their help with live-cell imaging. This work was supported by Medical Research Council core funding from the MRC-UCL University Unit Grant (Ref MC_U12266B) and funding from CRUK grant C37/A18784.

AUTHOR CONTRIBUTIONS

Conceptualization, G.A.W., K.V., G.S., S.A., C.B., and R.A.M.d.B.; methodology, G.A.W., K.V., C.B., and R.A.M.d.B.; investigation, G.A.W., K.V., G.S., C.H., L.M., J.C.-H., T.B., and R.J.M.; writing – original draft, G.A.W. and. R.A.M.d.B.; writing – review & editing, K.V. and R.A.M.d.B.; funding acquisition, M.T., S.A., and R.A.M.d.B.; resources, G.S., J.L., and S.A.; visualization, G.A.W., K.V., and R.A.M.d.B.; supervision, J.K.-V., M.T., S.A., C.B., and R.A.M.d.B.

DECLARATION OF INTERESTS

S.A. is an inventor on a patent describing samuraciclib, which is licensed to Carrick Therapeutics Ltd. S.A. has received royalties from and has share ownership in Carrick Therapeutics. J.L. is currently a full-time employee of and owns stock in Janssen Research and Development and is entitled to receive royalty payments for commercial use of cell lines described in this work under a licensing agreement between Johns Hopkins University and Horizon Discovery, Ltd.

INCLUSION AND DIVERSITY

We support inclusive, diverse, and equitable conduct of research.

Received: September 15, 2022
Revised: July 25, 2023
Accepted: October 16, 2023
Published: November 16, 2023

REFERENCES

1. Matthews, H.K., Bertoli, C., and de Bruin, R.A.M. (2022). Cell cycle control in cancer. Nat. Rev. Mol. Cell Biol. *23*, 74–88. https://doi.org/10.1038/s41580-021-00404-3.
2. Sava, G.P., Fan, H., Coombes, R.C., Buluwela, L., and Ali, S. (2020). CDK7 inhibitors as anticancer drugs. Cancer Metastasis Rev. *39*, 805–823. https://doi.org/10.1007/s10555-020-09885-8.
3. Patel, H., Periyasamy, M., Sava, G.P., Bondke, A., Slafer, B.W., Kroll, S.H.B., Barbazanges, M., Starkey, R., Ottaviani, S., Harrod, A., et al. (2018). ICEC0942, an orally bioavailable selective inhibitor of CDK7 for cancer treatment. Mol. Cancer Ther. *17*, 1156–1166. https://doi.org/10.1158/1535-7163.MCT-16-0847.
4. Sava, G.P., Fan, H., Fisher, R.A., Lusvarghi, S., Pancholi, S., Ambudkar, S.V., Martin, L.A., Charles Coombes, R., Buluwela, L., and Ali, S. (2020). ABC-transporter upregulation mediates resistance to the CDK7 inhibitors

THZ1 and ICEC0942. Oncogene *39*, 651–663. https://doi.org/10.1038/s41388-019-1008-y.

5. Carrick Therapeutics (2021). Carrick Therapeutics receives FDA fast track designations for two samuraciclib combinations for the treatment of HR+, HER2lJ advanced breast cancer and locally advanced or metastatic triple negative breast cancer. https://www.carricktherapeutics.com/news-media/press-releases/detail/10/carrick-therapeutics-receives-fda-fast-track-designations.
6. Kwiatkowski, N., Zhang, T., Rahl, P.B., Abraham, B.J., Reddy, J., Ficarro, S.B., Dastur, A., Amzallag, A., Ramaswamy, S., Tesar, B., et al. (2014). Targeting transcription regulation in cancer with a covalent CDK7 inhibitor. Nature *511*, 616–620. https://doi.org/10.1038/nature13393.
7. Olson, C.M., Liang, Y., Leggett, A., Lin, C.Y., Kwiatkowski, N., Gray, N.S., Park, W.D., Li, L., Mills, C.E., Elsarrag, S.Z., et al. (2019). Development of a selective CDK7 covalent inhibitor reveals predominant cell-cycle phenotype article development of a selective CDK7 covalent inhibitor reveals predominant cell-cycle phenotype. Cell Chem. Biol. *26*, 792–803.e10. https://doi.org/10.1016/j.chembiol.2019.02.012.
8. Vichai, V., and Kirtikara, K. (2006). Sulforhodamine B colorimetric assay for cytotoxicity screening. Nat. Protoc. *1*, 1112–1116. https://doi.org/10.1038/nprot.2006.179.
9. van Meerloo, J., Kaspers, G.J.L., and Cloos, J. (2011). Cell sensitivity assays: the MTT assay. In Cancer Cell Culture (Springer), pp. 237–245. https://doi.org/10.1007/978-1-61779-080-5_20.
10. Lolli, G., and Johnson, L.N. (2005). CAK-Cyclin-dependent activating kinase: a key kinase in cell cycle control and a target for drugs? Cell Cycle *4*, 572–577. https://doi.org/10.4161/cc.4.4.1607.
11. Fisher, R.P. (2012). The CDK network: linking cycles of cell division and gene expression. Genes Cancer *3*, 731–738. https://doi.org/10.1177/1947601912473308.
12. Schachter, M.M., Merrick, K.A., Larochelle, S., Hirschi, A., Zhang, C., Shokat, K.M., Rubin, S.M., and Fisher, R.P. (2013). A Cdk7-Cdk4 T-loop phosphorylation cascade promotes G1 progression. Mol. Cell *50*, 250–260. https://doi.org/10.1016/j.molcel.2013.04.003.
13. Schwartz, G.K., and Shah, M.A. (2005). Targeting the cell cycle: a new approach to cancer therapy. J. Clin. Oncol. *23*, 9408–9421. https://doi.org/10.1200/JCO.2005.01.5594.
14. Sakaue-Sawano, A., Kurokawa, H., Morimura, T., Hanyu, A., Hama, H., Osawa, H., Kashiwagi, S., Fukami, K., Miyata, T., Miyoshi, H., et al. (2008). Visualizing spatiotemporal dynamics of multicellular cell-cycle progression. Cell *132*, 487–498. https://doi.org/10.1016/j.cell.2007.12.033.
15. Herranz, N., and Gil, J. (2018). Mechanisms and functions of cellular senescence. J. Clin. Invest. *128*, 1238–1246. https://doi.org/10.1172/JCI95148.
16. Debacq-Chainiaux, F., Erusalimsky, J.D., Campisi, J., and Toussaint, O. (2009). Protocols to detect senescence-associated beta-galactosidase (SA-βgal) activity, a biomarker of senescent cells in culture and in vivo. Nat. Protoc. *4*, 1798–1806. https://doi.org/10.1038/nprot.2009.191.
17. Cahu, J., and Sola, B. (2013). A sensitive method to quantify senescent cancer cells. J. Vis. Exp. https://doi.org/10.3791/50494.
18. Kohli, J., Wang, B., Brandenburg, S.M., Basisty, N., Evangelou, K., Varela-Eirin, M., Campisi, J., Schilling, B., Gorgoulis, V., and Demaria, M. (2021). Algorithmic assessment of cellular senescence in experimental and clinical specimens. Nat. Protoc. *16*, 2471–2498. https://doi.org/10.1038/s41596-021-00505-5.
19. Freund, A., Laberge, R.M., Demaria, M., and Campisi, J. (2012). Lamin B1 loss is a senescence-associated biomarker. Mol. Biol. Cell *23*, 2066–2075. https://doi.org/10.1091/mbc.E11-10-0884.
20. Bertomeu, T., Coulombe-Huntington, J., Chatr-aryamontri, A., Bourdages, K.G., Coyaud, E., Raught, B., Xia, Y., and Tyers, M. (2018). A high-resolution genome-wide CRISPR/Cas9 viability screen reveals structural features and contextual diversity of the human cell-essential proteome. Mol. Cell. Biol. *38*. https://doi.org/10.1128/MCB.00302-17.
21. Eden, E., Lipson, D., Yogev, S., and Yakhini, Z. (2007). Discovering motifs in ranked lists of DNA sequences. PLoS Comput. Biol. *3*, e39. https://doi.org/10.1371/journal.pcbi.0030039.
22. Eden, E., Navon, R., Steinfeld, I., Lipson, D., and Yakhini, Z. (2009). GOrilla: a tool for discovery and visualization of enriched GO terms in ranked gene lists. BMC Bioinformatics *10*, 48. https://doi.org/10.1186/1471-2105-10-48.
23. Supek, F., Bošnjak, M., Škunca, N., and Šmuc, T. (2011). REVIGO summarizes and visualizes long lists of gene ontology terms. PLoS One *6*, e21800. https://doi.org/10.1371/journal.pone.0021800.
24. Chauvin, C., Koka, V., Nouschi, A., Mieulet, V., Hoareau-Aveilla, C., Dreazen, A., Cagnard, N., Carpentier, W., Kiss, T., Meyuhas, O., et al. (2014). Ribosomal protein S6 kinase activity controls the ribosome biogenesis transcriptional program. Oncogene *33*, 474–483. https://doi.org/10.1038/onc.2012.606.
25. Klingebiel, M., Dinekov, M., and Köhler, C. (2017). Analysis of ribosomal protein S6 baseline phosphorylation and effect of tau pathology in the murine brain and human hippocampus. Brain Res. *1659*, 121–135. https://doi.org/10.1016/j.brainres.2017.01.016.
26. Thoreen, C.C., Kang, S.A., Chang, J.W., Liu, Q., Zhang, J., Gao, Y., Reichling, L.J., Sim, T., Sabatini, D.M., and Gray, N.S. (2009). An ATP-competitive mammalian target of rapamycin inhibitor reveals rapamycin-resistant functions of mTORC1. J. Biol. Chem. *284*, 8023–8032. https://doi.org/10.1074/jbc.M900301200.
27. Demidenko, Z.N., and Blagosklonny, M.V. (2008). Growth stimulation leads to cellular senescence when the cell cycle is blocked. Cell Cycle *7*, 3355–3361. https://doi.org/10.4161/cc.7.21.6919.
28. Blagosklonny, M.V. (2012). Cell cycle arrest is not yet senescence, which is not just cell cycle arrest: terminology for TOR-driven aging. Aging *4*, 159–165.
29. Terzi, M.Y., Izmirli, M., and Gogebakan, B. (2016). The cell fate: senescence or quiescence. Mol. Biol. Rep. *43*, 1213–1220. https://doi.org/10.1007/s11033-016-4065-0.
30. Neurohr, G.E., Terry, R.L., Lengefeld, J., Bonney, M., Brittingham, G.P., Moretto, F., Miettinen, T.P., Vaites, L.P., Soares, L.M., Paulo, J.A., et al. (2019). Excessive cell growth causes cytoplasm dilution and contributes to senescence. Cell *176*, 1083–1097.e18. https://doi.org/10.1016/j.cell.2019.01.018.
31. Hollestelle, A., Nagel, J.H.A., Smid, M., Lam, S., Elstrodt, F., Wasielewski, M., Ng, S.S., French, P.J., Peeters, J.K., Rozendaal, M.J., et al. (2010). Distinct gene mutation profiles among luminal-type and basal-type breast cancer cell lines. Breast Cancer Res. Treat. *121*, 53–64. https://doi.org/10.1007/s10549-009-0460-8.
32. Smith, S.E., Mellor, P., Ward, A.K., Kendall, S., McDonald, M., Vizeacoumar, F.S., Vizeacoumar, F.J., Napper, S., and Anderson, D.H. (2017). Molecular characterization of breast cancer cell lines through multiple omic approaches. Breast Cancer Res. *19*, 65. https://doi.org/10.1186/s13058-017-0855-0.
33. Dimri, G.P. (2005). What has senescence got to do with cancer? Cancer Cell *7*, 505–512. https://doi.org/10.1016/j.ccr.2005.05.025.
34. Liu, S., Tang, Y., Yan, M., and Jiang, W. (2018). PIK3CA mutation sensitizes breast cancer cells to synergistic therapy of PI3K inhibition and AMPK activation. Invest. New Drugs *36*, 763–772. https://doi.org/10.1007/s10637-018-0563-3.
35. Tian, T., Li, X., and Zhang, J. (2019). mTOR Signaling in cancer and mTOR inhibitors in solid tumor targeting therapy. Int. J. Mol. Sci. *20*. https://doi.org/10.3390/ijms20030755.
36. Beaver, J.A., Gustin, J.P., Yi, K.H., Rajpurohit, A., Thomas, M., Gilbert, S.F., Rosen, D.M., Ho Park, B., and Lauring, J. (2013). PIK3CA and AKT1 mutations have distinct effects on sensitivity to targeted pathway inhibitors in an isogenic luminal breast cancer model system. Clin. Cancer Res. *19*, 5413–5422. https://doi.org/10.1158/1078-0432.CCR-13-0884.

37. Foy, R., Crozier, L., Pareri, A.U., Valverde, J.M., Park, B.H., Ly, T., and Saurin, A.T. (2023). Oncogenic signals prime cancer cells for toxic cell growth during a G1 cell cycle arrest. Mol. Cell *83*. https://doi.org/10.1101/2022.09.08.506962.

38. Peng, Y., Wang, Y., Zhou, C., Mei, W., and Zeng, C. (2022). PI3K/Akt/mTOR pathway and its role in cancer therapeutics: are we making headway? Front. Oncol. *12*, 819128. https://doi.org/10.3389/fonc.2022.819128.

39. Lengefeld, J., Cheng, C.W., Maretich, P., Blair, M., Hagen, H., McReynolds, M.R., Sullivan, E., Majors, K., Roberts, C., Kang, J.H., et al. (2021). Cell size is a determinant of stem cell potential during aging. Sci. Adv. *7*, eabk0271. https://doi.org/10.1126/sciadv.abk0271.

40. Lanz, M.C., Zatulovskiy, E., Swaffer, M.P., Zhang, L., Ilerten, I., Zhang, S., You, D.S., Marinov, G., McAlpine, P., Elias, J.E., et al. (2022). Increasing cell size remodels the proteome and promotes senescence. Mol. Cell *82*, 3255–3269.e8. https://doi.org/10.1016/j.molcel.2022.07.017.

41. Xie, S., Swaffer, M., and Skotheim, J.M. (2022). Eukaryotic cell size control and its relation to biosynthesis and senescence. Annu. Rev. Cell Dev. Biol. *38*, 291–319. https://doi.org/10.1146/annurev-cellbio-120219-040142.

42. Manohar, S., Estrada, M.E., Uliana, F., Vuina, K., Moyano Alvarez, P., de Bruin, R.A.M., and Neurohr, G.E. (2023). Genome homeostasis defects drive enlarged cells into senescence. Mol. Cell *83*. https://doi.org/10.17632/x5ypd2mk5g.1.

43. Crozier, L., Foy, R., Adib, R., Kar, A., Holt, J.A., Pareri, A.U., Valverde, J.M., Rivera, R., Weston, W.A., Wilson, R., et al. (2023). CDK4/6 inhibitor-mediated cell overgrowth triggers osmotic and replication stress to promote senescence. Mol. Cell *83*. https://doi.org/10.1016/j.molcel.2023.10.016.

44. Raab, M., Gentili, M., de Belly, H., Thiam, H.R., Vargas, P., Jimenez, A.J., Lautenschlaeger, F., Voituriez, R., Lennon-Duménil, A.M., Manel, N., et al. (2016). ESCRT III repairs nuclear envelope ruptures during cell migration to limit DNA damage and cell death. Science *352*, 359–362. https://doi.org/10.1126/science.aad7611.

45. Wang, T., Wei, J.J., Sabatini, D.M., and Lander, E.S. (2014). Genetic screens in human cells using the CRISPR-Cas9 system. Science *343*, 80–84. https://doi.org/10.1126/science.1246981.

46. Stewart, S.A., Dykxhoorn, D.M., Palliser, D., Mizuno, H., Yu, E.Y., An, D.S., Sabatini, D.M., Chen, I.S.Y., Hahn, W.C., Sharp, P.A., et al. (2003). Lentivirus-delivered stable gene silencing by RNAi in primary cells. RNA *9*, 493–501. https://doi.org/10.1261/rna.2192803.

47. Skehan, P., Storeng, R., Scudiero, D., Monks, A., McMahon, J., Vistica, D., Warren, J.T., Bokesch, H., Kenney, S., and Boyd, M.R. (1990). New colorimetric cytotoxicity assay for anticancer-drug screening. J. Natl. Cancer Inst. *82*, 1107–1112. https://doi.org/10.1093/jnci/82.13.1107.

48. Langmead, B., and Salzberg, S.L. (2012). Fast gapped-read alignment with Bowtie 2. Nat. Methods *9*, 357–359. https://doi.org/10.1038/nmeth.1923.

49. Benjamini, Y., and Hochberg, Y. (1995). Controlling the false discovery rate: a practical and powerful approach to multiple testing. J. R. Stat. Soc. B Methodol. *57*, 289–300. https://doi.org/10.1111/j.2517-6161.1995.tb02031.x.

STAR★METHODS

KEY RESOURCES TABLE

REAGENT or RESOURCE	SOURCE	IDENTIFIER
Antibodies		
Caspase 3	Cell Signaling Technology	Cat#9662; RRID: AB_331439
Phospho-CDK1 (Thr161)	Cell Signaling Technology	Cat#9114; RRID: AB_2074652
Phospho-Histone H2A.X (Ser139)	Cell Signaling Technology	Cat#9718; RRID: AB_2118009
Phospho-Chk2 (Thr68)	Cell Signaling Technology	Cat#2661; RRID: AB_331479
$p16^{INK4a}$	Abcam	Cat#ab108349; RRID: AB_10858268
$p21^{CIP1}$	Cell Signaling Technology	Cat#2947; RRID: AB_823586
Lamin B1	Abcam	Cat#ab16048; RRID: AB_443298
Phospho-Rb (Ser807/811)	Cell Signaling Technology	Cat#8516; RRID: AB_11178658
Rb	Cell Signaling Technology	Cat#9309; RRID: AB_823629
Phospho-RNA polymerase II CTD repeat YSPTSPS (Ser 5)	Abcam	Cat#ab5131; RRID: AB_449369
Phospho-p70 S6 kinase (Thr389)	Cell Signaling Technology	Cat#9234; RRID: AB_2269803
p70 S6 kinase	Cell Signaling Technology	Cat#2708; RRID: AB_390722
Phospho-S6 ribosomal protein (Ser235/236)	Cell Signaling Technology	Cat#2211; RRID: AB_331679
GAPDH	Genetex	Cat#GTX627408; RRID: AB_11174761
α-tubulin	Cell Signaling Technology	Cat#3873; RRID: AB_1904178
Vinculin	Abcam	Cat#ab129002; RRID: AB_11144129
Goat anti mouse IgG HRP conjugate	Thermo Fisher Scientific	Cat#PA1-74421; RRID:AB_10988195
Goat anti-rabbit IgG HRP conjugate	Thermo Fisher Scientific	Cat#31460; RRID: AB_228341
Alexa Fluor 647 goat anti-rabbit	Invitrogen	Cat#A21244; RRID: AB_2535812
Chemicals, peptides, and recombinant proteins		
Samuraciclib	Laboratory of Simak Ali	N/A
THZ1	Apex Bio	Cat#A8882 CAS 1604810-83-4
Torin1	Merck Millipore	Cat#475991 CAS 1222998-36-8
Etoposide	Sigma Aldrich	Cat#E1383 CAS 33419-42-0
Camptothecin	Sigma Aldrich	Cat#208925 CAS 7689-03-4
Bafilomycin A1	Sigma Aldrich	Cat#B1793 CAS 88899-55-2
5-dodecanoylaminofluorescein di-β-D-galactopyranoside (C_{12}FDG)	Invitrogen	Cat#D2893
Trichloroacetic acid	Sigma Aldrich	Cat#T0699 CAS 76-03-9
Sulforhodamine B (SRB) sodium salt	Sigma Aldrich	Cat#S9012 CAS 3520-42-1
Propidium iodide	Sigma Aldrich	Cat#P4864-10ML CAS 25535-16-4
Formaldehyde	Sigma Aldrich	Cat#252549 CAS 50-00-0
DAPI	Sigma Aldrich	Cat#D9564 CAS 28718-90-3
RNaseA	Sigma Aldrich	Cat#R4875 CAS 9001-99-4
Phosphatase inhibitor cocktail 2	Sigma Aldrich	Cat#P5726
Phosphatase inhibitor cocktail 3	Sigma Aldrich	Cat#P0044
Protease inhibitor cocktail	Sigma Aldrich	Cat#P8340
MOPS SDS Running Buffer (20X)	Invitrogen	Cat#NP0001
Immobilon Block-CH	Merck Millipore	Cat#WBAVDCH01

(*Continued on next page*)

Continued

REAGENT or RESOURCE	SOURCE	IDENTIFIER
Immobilon Crescendo Western HRP substrate	Merck Millipore	Cat#WBLUR0100
Fibronectin	Sigma Aldrich	Cat#F1141 EC 289-149-2
Triton X-100	Sigma Aldrich	Cat#T8787 CAS 9036-19-5
Hoechst	Invitrogen	Cat#H3570
Fluoroshield	Sigma Aldrich	Cat#F6182 CAS 55965-84-9
Critical commercial assays		
MTT Cell Growth Assay Kit	Millipore	Cat#CT02
Annexin V-iFluor 647 Apoptosis Detection Kit	Abcam	Cat#ab219919
Click-iT EdU Alexa Fluor 647 Flow Cytometry Assay Kit	Thermo Fisher Scientific	Cat#C10424
Senescence β-galactosidase staining kit	Cell Signaling Technology	Cat#9860
CellTiter-Glo Reagent	Promega	Cat#G7570
Gentra Puregene Cell kit	Qiagen	Cat#158745
TG NextSeq® 500/550 High Output Kit v2 (75 cycles)	Illumina	Cat#TG-160-2005
AxyPrep FragmentSelect-I Kit	Axygen	Cat#MAGFRAG-I-50
Deposited data		
Genome-wide CRISPR knockout chemogenetic screen data	This paper	GEO: GSE244434
Experimental models: Cell lines		
hTERT-RPE1	ATCC	CRL-4000
hTERT-RPE1-FUCCI	Laboratory of Buzz Baum	N/A
pre-B lymphoblastic human cell line: NALM-6	Laboratory of Stephen Elledge	N/A
pre-B lymphoblastic human NALM-6 Cas9 clone #20	Bertomeu et al.[20]	N/A
pre-B lymphoblastic human NALM-6 Cas9 clone #20 transduced with the EKO library	Bertomeu et al.[20]	N/A
MCF7	ATCC	HTB-22
T47D	ATCC	HTB-133
BT549	ATCC	HTB-122
MCF7 *PIK3CA*^{mut}	Laboratory of Josh Lauring, Beaver et al.[36]	N/A
MCF7 *PIK3CA*^{wt}	Laboratory of Josh Lauring, Beaver et al.[36]	N/A
MCF7 *PIK3CA*^{mut} expressing nuclear EGFP	Laboratory of Simak Ali	N/A
MCF7 *PIK3CA*^{wt} expressing nuclear EGFP	Laboratory of Simak Ali	N/A
Oligonucleotides		
Outer 1: AGCGCTAGCTAATGCCAACTT	Bertomeu et al.[20]	N/A
Outer 2: GCCGGCTCGAGTGTACAAAA	Bertomeu et al.[20]	N/A
TruSeq Univestal adapter +0: AATGATACGG CGACCACCGAGATCTACACTCTTTCCCTACACGA CGCTCTTCCGATCTCTTGTGGAAAGGACGAAACA	Bertomeu et al.[20]	N/A
TruSeq Adapter with index: CAAGCAGAAGACGGCA TACGAGAT(6bp index)GTGACTGGAGTTCAGACGTG TGC TCTTCCGATCCACCGACTCGGTGCCACTTTT	Bertomeu et al.[20]	N/A
Recombinant DNA		
pTRIP-SFFV-EGFP-NLS	Raab et al.[44]	Addgene: #86677
pLX-sgRNA	Wang et al.[45]	Addgene: #50662
pCW-Cas9	Wang et al.[45]	Addgene: #50661
psPAX2	Laboratory of Didier Trono	Addgene: #12260

(*Continued on next page*)

Continued

REAGENT or RESOURCE	SOURCE	IDENTIFIER
pCMV-VSV-G	Stewart et al.[46]	Addgene: #8454
EKO (Extended knock-out) plasmidic library in pLX-sgRNA	Bertomeu et al.[20]	N/A
Software and algorithms		
FlowJo	BD Biosciences RRID:SCR_008520	https://www.flowjo.com/solutions/flowjo
FIJI	ImageJ RRID:SCR_002285	https://imagej.nih.gov/ij/index.html
GraphPad Prism	GraphPad Software Inc RRID:SCR_002798	https://www.graphpad.com/scientific-software/prism/
GOrilla: Gene Ontology Enrichment Analysis and Visualization Tool	GOrilla RRID:SCR_006848	http://cbl-gorilla.cs.technion.ac.il/

RESOURCE AVAILABILITY

Lead Contact

Further information and requests for resources and reagents should be directed to and will be fulfilled by the lead contact, Robertus A.M. de Bruin (r.debruin@ucl.ac.uk).

Materials availability

Material generated in this study can be made available upon request from the lead contact.

Data and code availability

- Genome-wide CRISPR knockout chemogenetic screen data have been deposited on GEO and are publicly available as of the date of publication. Accession number is listed in the key resources table. All other raw data will be shared by the lead contact upon request.
- This paper does not report original code.
- Any additional information required to reanalyse the data reported in this paper is available from the lead contact upon request.

EXPERIMENTAL MODEL AND STUDY PARTICIPANT DETAILS

Cell lines used were immortalized hTERT human Retinal Pigment Epithelial 1 (RPE1) (ATCC CRL-4000), hTERT-RPE1-FUCCI cells (a gift from Buzz Baum, MRC LMB, Cambridge, UK), NALM-6 cells (a gift from Stephen Elledge, Harvard Medical School, Boston, MA, USA), MCF7 cells (ATCC HTB-22), T47D (HTB-133) and BT549 (HTB-122) cells. The pair of isogenic MCF7 cell lines, with and without *PIK3CA* mutation, were published previously and created by somatic gene targeting to correct the native E545K mutation in *PIK3CA* as previously described.[36]

Retinal Pigment Epithelial 1 cells were cultured in DMEM/F12 media supplemented with 10% fetal bovine serum (Sigma Aldrich), 1% penicillin/streptomycin (Gibco) and 3% sodium bicarbonate (Gibco). NALM-6, T47D and BT549 cells were cultured in RPMI media supplemented with 10% fetal bovine serum (Sigma Aldrich) and 1% penicillin/streptomycin (Gibco). MCF7 cells were cultured in DMEM media supplemented with 10% fetal bovine serum (Sigma Aldrich) and 1% penicillin/streptomycin (Gibco). All cells were cultured at 37°C with 5% CO_2.

The pair of isogenic MCF7 cell lines, with and without *PIK3CA* mutation, were made to stably express nuclear EGFP, by lentiviral transduction of pTRIP-SFFV-EGFP-NLS (Addgene, #86677) packaged in HEK293T cells, to allow for accurate quantification of cell number via IncuCyte Zoom.

METHOD DETAILS

Drug treatments

Cells were treated with samuraciclib at the specified final concentrations, with etoposide (Sigma Aldrich, E1383) (0.5 μg/ml), with camptothecin (Sigma Aldrich, 208925) (2 μM) with Bafilomycin A1 (Sigma Aldrich, B1793) 1 hour prior to 5-dodecanoylaminofluorescein di-β-D-galactopyranoside (C_{12}FDG) addition (100 nM), with Torin1 (Merck Millipore, 475991) (25 nM) and with THZ1 (Apex Bio, A882) (50 nM). DMSO (Sigma Aldrich, D2438) was the vehicle control in each experiment and the highest concentration used was 0.0012% of total volume.

Cell proliferation and viability

To determine the GI_{50} concentration of samuraciclib, cell number in response to drug treatment was assessed using the sulforhodamine B (SRB) assay.[47] Cells were left to adhere for 48 hours at 37°C and 5% CO_2. After 48 hours, serial dilutions of samuraciclib were added to the well, with final concentrations of the compounds ranging from 20 μM to 0.076 nM. DMSO was added as a control at a final concentration of 0.001%. On the same day a control seeding plate was fixed to allow quantification of cell growth. The cells were incubated with the range of compound dilutions for 48 hours. After 48 hours, cells were fixed with 40% Trichloroacetic acid (Sigma Aldrich, T0699) and then incubated with SRB sodium salt (Sigma Aldrich, S9012) (0.4% in 1% acetic acid) for 1 hour at room temperature. After air drying, 10 mM Tris base was added to the cells and absorbance was measured at 492 nm on a VersaMax Tunable Microplate Reader (Molecular Devices). The data was then analysed to determine the percentage growth compared to the seeding plate fixed prior to addition of compound dilutions.

To assess cell viability, the MTT assay was carried out using the MTT Cell Growth Assay Kit (Millipore, CT02) following manufacturer's instructions. Cells were incubated with the MTT (3-(4,5-dimethylthiazol-2-yl)-2,5-diphenyl tetrazolium bromide) solution for 2-4 hours at 37°C, before the precipitate that formed was dissolved using 0.04 N HCl in isopropanol. Absorbance was measured at 570 nm on a VersaMax Tunable Microplate Reader (Molecular Devices).

To determine the response of the pair of isogenic MCF7 cell lines, with and without *PIK3CA* mutation, expressing nuclear EGFP to drug treatment for 30 days, plates were imaged using an IncuCyte Zoom every 3 days and nuclear EGFP was used to assess cell numbers. Culture medium and drugs were replenished every 3 days.

Flow cytometry

For analysis of Annexin V/propidium iodide (PI), cells were collected by trypsinisation, and Annexin V staining was carried out using an Annexin V-iFluor 647 Apoptosis Detection Kit (Abcam, ab219919), following manufacturer's instructions. Cells were trypsinised and washed with PBS. They were then incubated in Assay buffer containing the Annexin-V iFluor 647 conjugate for 30 minutes at room temperature. After this, PI (Sigma Aldrich, P4864-10ML) was added to each sample at a final concentration of 10 μg/ml and the cells were then analysed by flow cytometry.

For analysis of EdU/DAPI, EdU was added to the cell culture media at the final concentration of 10 μM and cells were incubated for 1 hour at 37°C with 5% CO_2. Cells were trypsinised and resuspended in PBS and then fixed in 4% Formaldehyde (Sigma Aldrich, 252549) for 15 minutes at room temperature. EdU detection was then performed using Click-iT EdU Alexa Fluor 647 Flow Cytometry Assay Kit (Thermo Fisher, C10424) following manufacturer's instructions. Prior to EdU detection, cells were counted and diluted to the same number in each sample. Cells were washed in 1 mg/ml BSA in PBS and resuspended in saponin-based permeabilization and wash reagent at room temperature for 15 minutes. Cells were then resuspended in Analysis buffer and incubated at room temperature for 30 minutes. After this, cells were incubated in 0.5 μg/ml DAPI (Sigma Aldrich, D9564) for at least 15 minutes at room temperature and then analysed.

For analysis of DNA content by PI staining, cells were trypsinised and fixed in 70% ethanol at -20°C overnight. After centrifugation, the cell pellet was washed with PBS. Cells were then incubated in 350 μl PBS with 100 μg/ml RNaseA (Sigma Aldrich, R4875) and 50 μg/ml PI overnight at 4°C.

For analysis of SA β-gal activity, flow cytometry was carried out as previously described in Debacq-Chainiaux et al.[16] and Cahu and Sola[17]. Prior to cell collection, the cell's media was changed, and cells were incubated with Bafilomycin A1 at a final concentration of 100 nM for 1 hour at 37°C. After this, the cells were incubated with C_{12}FDG (Invitrogen, D2893) at a final concentration of 33 μM for 2 hours at 37°C. The cells were then trypsinised and centrifuged at 300 xg for 5 minutes at 4°C. The cell pellets were resuspended in 500 μl of ice-cold PBS and analysed by flow cytometry.

For all experiments using the flow cytometer, samples were measured on a BD LSRII flow cytometer using DIVA software (BD) and analysed using FlowJo software.

Western blot

Cell extracts were prepared in RIPA buffer (Tris pH 7.5 20 mM, NaCl 150 mM, EDTA 1 mM, EGTA 1 mM, NP-40 1%, NaDoc 1%), phosphatase inhibitor cocktail 2 and 3 (Sigma Aldrich P5726 and P0044) 1:1000, and protease inhibitor cocktail (Sigma Aldrich P8340) 1:1000. Proteins were separated on NuPAGE Novex 4-12% Bis-Tris protein gels (Invitrogen, NP0322) in MOPS running buffer (Invitrogen, NP0001) and transferred onto nitrocellulose membrane (Sigma, GE10600001) by wet transfer in transfer buffer (25 mM Tris base, 250 mM glycine, 10% ethanol). Membranes were blocked in 5% milk dissolved in PBS/0.2% Tween or in Immobilon Block-CH reagent (Merck Millipore, WBAVDCH01) for 1 hour at room temperature. Membranes were then incubated in primary antibodies overnight at 4°C. Following PBS/0.2% Tween washes, membranes were incubated in secondary HRP antibodies for 1-2 hours at room temperature. HRP was visualised using Immobilon Crescendo Western HRP substrate (Merck Millipore, WBLUR0100).

Primary antibodies used were anti Caspase 3 (Cell Signaling Technology 9662 rabbit 1:1000), anti Phospho-CDK1 (Thr161) (Cell Signaling Technology 9114 rabbit 1:100), anti Phospho-Histone H2A.X (γH2AX) (Ser139) (Cell Signaling Technology 9718 rabbit 1:250), anti Phospho-Chk2 (Thr68) (Cell Signaling Technology 2661 rabbit 1:500), anti $p16^{INK4a}$ (Abcam ab108349 rabbit 1:2000), anti $p21^{CIP1}$ (Cell Signaling Technology 2947 rabbit 1:2000), anti-Lamin B1 (Abcam ab16048, rabbit, 1:5000), anti Phospho-Rb (Ser807/811) (Cell Signaling Technology 8516 rabbit 1:1000), anti Rb (Cell Signaling Technology 9309, mouse 1:500), anti

Phospho-RNA polymerase II CTD repeat YSPTSPS (Ser5) (Abcam ab5131 rabbit 1:5000), anti Phospho-p70 S6 kinase (Thr389) (Cell Signaling Technology 9234 rabbit 1:1000), anti p70 S6 kinase (Cell Signaling Technology 2708 rabbit 1:1000), anti Phospho-S6 ribosomal protein (Ser235/236) (Cell Signaling Technology 2211 rabbit 1:1000). GAPDH (Genetex GTX627408 mouse 1:10000), α-tubulin (Cell Signaling Technology 3873 mouse 1:20,000) and vinculin (Abcam ab129002 rabbit 1:20,000) were used as loading controls. Secondary antibodies used were goat anti-mouse IgG HRP conjugate (Thermo Fisher Scientific PA1-74421 1:4000) and goat anti rabbit IgG HRP conjugate (Thermo Fisher Scientific 31460 1:4000).

Immunofluorescence

Cells were plated on coverslips precoated with fibronectin (Sigma Aldrich, F1141). Cells were fixed in 4% Formaldehyde (Sigma Aldrich, 252549) for 20 minutes at room temperature and then permeabilised with 0.2% Triton X-100 (Sigma Aldrich, T8787) in 1x PBS for 5 minutes at room temperature. Cells were blocked in 1% BSA 0.2% Tween in PBS for 1 hour at room temperature and incubated in primary antibody, anti Phospho-Histone H2A.X (γH2AX) (Ser139) (Cell Signaling Technology 9718 rabbit 1:1000), overnight at 4°C. Coverslips were incubated the following day in secondary antibody (Alexa Fluor 647 goat anti-rabbit, Invitrogen A21244, 1:2000) for 2 hours at room temperature. Coverslips were stained with Hoechst (Invitrogen, H3570), 1:10000 in 1x PBS and mounted on slides with Fluoroshield (Sigma Aldrich, F6182). Images were acquired with Leica SPE2 confocal microscope using a 40x objective lens and processed with Fiji. 100 cells were analysed per sample.

Detection of senescence-associated β-galactosidase activity

For detection of SA β-gal activity, cells were stained using a Senescence β-galactosidase staining kit (Cell Signaling Technology, 9860) following manufacturer's instructions. Cells were fixed with 1X fixative solution for 15 minutes at room temperature. After washing with PBS, cells were incubated in 1.5 ml of β-galactosidase staining solution overnight at 37°C in the absence of supplemented CO_2. All images were acquired with a Leica DM IRB microscope using a 10x objective lens.

Quantification of cell volume

For analysis of cell volume, cells were trypsinised and resuspended in culture media. They were then diluted 1:10 in Coulter Isoton II diluent (Beckman Coulter, 8546719) and cell volumes determined using a particle sizing and counting analyser (Multisizer 4 Coulter counter, Beckman Coulter) with Multisizer 4 software.

Live-cell imaging and analysis

hTERT-RPE1-FUCCI cells were used for live-cell imaging. For samuraciclib treatment experiment, hTERT-RPE1-FUCCI cells were plated in a 6-well plate one day prior to the start of the experiment. The following day cells were treated with vehicle control (DMSO) or samuraciclib and imaging was started for 48 hours. For samuraciclib wash-out/release experiment, hTERT-RPE1-FUCCI cells were treated with vehicle control (DMSO) or samuraciclib for 72 hours. Cells were then washed five times with PBS and fresh media was added after which imaging was started for 72 hours.

Live-cell imaging was performed on a Nikon Ti inverted microscope stand with a Nikon DS-Qi2 high sensitivity scientific CMOS camera using a 20x objective lens. Fluorescence filter sets were Nikon GFP HQ and Texas Red cubes. Fluorescence light source was a CoolLED pE-300. The Nikon DS-Qi2 camera acquisition was binned 3x to enhance sensitivity. Phase contrast and fluorescence images were taken every 10 minutes. Cells were maintained at 37°C with 5% CO_2.

Time-lapse movies were analysed manually by single cell tracking and determining the time of colour changes between red, yellow, green and loss of colour of FUCCI cells. Manual analysis could have resulted in slight differences in colour switch timings. Only cells that were in the field of view throughout the entire movie were included in the analysis and the daughter cells inherited the mother's track history. Therefore, a mother cell that divided once was presented as two single cell cycle FUCCI profile tracks and was counted as two cell cycle states. For the wash-out/release experiment, red cells were marked at the first timepoint and tracked. Cell cycle entry after samuraciclib wash-out was determined by yellow colour switch. Nuclear area was calculated in Fiji after nuclear segmentation using Bernsen local thresholding.

Genome-wide CRISPR knock-out chemogenetic screen

sgRNAs pooled library generation

The pooled library of 278, 754 different sgRNAs called EKO (extended-knockout) was inserted within the pLX-sgRNA plasmid (Addgene #50662) and lentivirus was generated in HEK-293T cells as previously described.[20] A doxycycline-inducible Cas9 clonal cell line of NALM-6 (using plasmid pCW-Cas9, Addgene #50661) was generated, infected with the pooled lentivirus libraries and underwent blasticidin selection as previously described.

Proliferation assay

To determine the IC_{30} concentration of samuraciclib in NALM-6 cells, a Beckman Coulter BioMek FX robot was used to mix NALM-6 cells with 11 different concentrations of the drugs (1:3 dilutions) and they were then loaded into 384-well plates, keeping solvent concentration constant (0.1%) across all wells (IRIC's HTS platform, Montréal, Canada). Plates were kept for 3 days in a high humidity chamber installed in a 37°C 5% CO_2 incubator. 50 μl of CellTiter-Glo reagent (Promega) was then added, plates were shaken for 2 minutes, and luminescence read on a BioTek Synergy/Neo microplate reader.

Chemogenetic screen

A NALM-6 doxycycline-inducible Cas9 clone previously infected and blasticidin-selected following lentiviral infection with EKO lentivirus (MOI of 0.3 and a representation of at least 500 cells per sgRNA) was thawed (representation of at least 250 cells per sgRNA) and treated with 2 μg/ml doxycycline to induce Cas9 expression 7 days before samuraciclib was added. Prior to drug addition, a minimum of 70 million cells were collected as samples that had had doxycycline added but had not been treated with drugs. The remaining cells were diluted to 400 000 cells per mL. 28 million cells (100 cells per sgRNA) were treated with 350 nM samuraciclib (the IC_{30} concentration) and 70 million cells were treated with 0.1% DMSO. A minimum of 70 million cells were left untreated as control. Cell concentration was monitored every 2 days by diluting 1 ml of the cells 1:10 in Isoton II diluent and using a Beckman Coulter Z2 particle count and size analyser. The cells were diluted accordingly to prevent cells from arresting and compounds or DMSO added to maintain initial concentration. After 8 days, the different populations of cells were pelleted, washed with PBS and frozen.

Next Generation Sequencing

Genomic DNA extractions were done using the Gentra Puregene Cell kit (Qiagen). sgRNA sequences were amplified by PCR using 462 μg of genomic DNA (corresponding to 70 million cells), 575 μL 10X reaction buffer, 115 μl 10 mM dNTPs, 23 μl 100 μM primer Outer 1, 23 μl 100 μM primer Outer 2, 115 μl DMSO and 145 units of GenScript Green Taq DNA polymerase in a total volume of 5.75 mL or 185 μg (28 million cells; same PCR recipe in 2.5X smaller volumes) as templates. Whenever DNA quantities requirements were not met, everything was used and a corresponding few more cycles performed. Multiple 100 μl reactions were set up in 96-well formats on a BioRad T100 thermal cycler and the steps were as follows: 95°C 5 minutes, 25 cycles of 35 seconds at 94°C, 35 seconds at 52°C and 36 seconds at 72°C, final step of 10 minutes at 72°C after the last cycle. Completed 100 μl reaction mixes were combined into one tube and vortexed and 1.5 mL aliquots were concentrated to 100 μl by ethanol-precipitation.

A second PCR reaction was performed to add Illumina sequencing adapters and 6 bp indexing primers, using 10 μl of 1:20 dilution of unpurified PCR1 product, 10 μl 5X buffer Kapa, 5 μl 2,5 mM dNTPs, 1 μl of PAGE-purified equimolar premix 100 μM TruSeq Universal Adapter 0, 1 μl of 100 μM PAGE-purified TruSeq Adapter with appropriate index, 1 μl DMSO and 5 units Kapa HiFi HotStart DNA polymerase and volumes brought to 50 μl total volume. The steps of the PCR reaction were as follows: 5 minutes at 95°C, 5 cycles of 15 seconds at 95°C, 30 seconds at 50°C and 30 seconds at 72°C, 5 cycles of 15 seconds at 95°C, 30 seconds at 56°C and 30 seconds at 72°C, followed by 5 minutes final step at 72°C after the last cycle. A 238-239 bp amplicon was purified using a 1:1 ratio of Spry beads (AxyPrep Mag FragmentSelect-I, Axygen) and 45 bp was read on an Illumina NextSeq 500 with the 23 first bp read in dark cycles (IRIC's genomic platform, Montréal, Canada). Sequencing coverage was close to 20 samples per lane.

QUANTIFICATION AND STATISTICAL ANALYSIS

GraphPad Prism was used to carry out statistical analysis. Statistical details for each analysis can be found in the figure legends and figures. Statistical tests used and the number of independent experiments are indicated in figure legends.

Key for statistical analysis used throughout: ns=$P > 0.05$, *=$P < 0.05$, **=$P < 0.01$, ***=$P < 0.001$, ****=$P < 0.0001$.

For the chemogenetic screen, reads were aligned using Bowtie2.2.5[48] in the forward direction only (-norc option) with otherwise default parameters and total read counts per sgRNA tabulated. Read counts from the different time-points of the control screens were summed, including untreated, 0.1% DMSO-treated and 0.1% ethanol-treated samples, to generate a single reference sgRNA distribution. Gene scores were calculated using the RANKS tool,[20] with a minimal read threshold of 200 and otherwise default settings. Statistical analysis of Gene Ontology (GO) enrichment was carried out using GOrilla, a web-based GO analysis tool.[21,22] The REVIGO web server was used to produce a representative sub-set of GO terms.[23] The FDR q-value is the corrected p-value using the Benjamini and Hochberg method.[21,22,49]

The enrichment value is defined as enrichment = (b/n) / (B/N) where:

- N=the total number of genes
- B=the total number of genes associated with a specific GO term
- n=the number of genes in the target set
- b=the number of genes in the intersection[21,22]